IEET
International Electrical Engineering Transactions

Vol. 6 No.1 (10)
January- June, 2020
ISSN 2465-4256

An online publication of the EEAAT
Electrical Engineering Academic Association (Thailand)
www.journal.eeaat.or.th

IEET – International Electrical Engineering Transactions

This journal is an online publication of the EEAAT, Electrical Engineering Academic Association (Thailand). IEET is published twice a year, ie., the first issue is for January – June and the second issue is for July – December.

EEAAT Journal Committee

IEET Editor

IEET (International Electrical Engineering Transactions) is published twice a year. Original contributions covering work in all aspects of electrical science, technology, engineering, and applications will be peer-reviewed by experts before publication. Topics of interest include the following: electrical power, electronics, telecommunication, control and system, sensor and measurement, optical technology, computer, information and communication technology (ICT), signal processing, social network tools and applications (apps), engineering education and other related fields.

For online submission of all manuscripts, correspondences, and letters, please visit
www.journal.eeaat.or.th

IEET Editorial Office

EEAAT - Electrical Engineering Academic Association (Thailand)
Room 409, F-Building,140 Cheum-Sampan Rd.
Nong Chok, Bangkok, Thailand 10530
Tel: +662-988-3655 ext 2216 Fax: +662-988-4026

IEET - International Electrical Engineering Transactions

Volume 6 (10)
Number 1
January – June 2020

PAPERS

Simulation of COVID-19 Epidemic Scenario in Thailand with SIR Model and Changeable Number of Populations

Suwit Kiravittaya*
Department of Electrical and Computer Engineering,
Faculty of Engineering, Naresuan University,
Phitsanulok, Thailand

Abstract: A method to simulate and fit the evolution dynamics of the COVID-19 epidemics in Thailand during January – April 2020 is explained. Based on a conventional Susceptible-Infected-Recovered (SIR) model and the reported data, we propose a time-varying form of the total population $N(t)$ in order to represent the realistic situation in the model. The SIR model is modified with gradually decreasing (after the outbreak) and abruptly increasing of $N(t)$. These considerations can improve the fitting results and thus enhance the understanding of the epidemic situation in Thailand. Extracted model parameter can be used to quantify the degree of the disease spreading. Finally, the reported world data is considered, and it can be qualitatively described with the proposed model.

***Index Terms*—Numerical Simulation, COVID-19, Susceptible-Infected-Recovered Model, Population, Thailand.**

I. Introduction

In the first quarter of 2020, an infectious disease named COVID-19 is spread globally. The human-to-human transmission ability of the coronavirus (SARS-CoV-2) and its severity affect human being in many aspects. The disease spreading is first noticed in the late 2019 [1]. In January 2020, the virus spreads over many countries including Thailand. On 13th January, the first infected case (Chinese lady) outside China is confirmed in Thailand. Then, the finding of the first infected Thai person, who has returned from China, is reported on 15th January [2]. After that, the numbers of infected cases as well as recovered cases gradually increase. On 12th March 2020, World Health Organization (WHO) announced the COVID-19 as a global pandemic as it rapidly spreads in all continents. At this time (22nd April 2020), the worldwide number of infected cases is more than 2.5 million and the death cases of nearly 200,000 are reported [3]. For the time being, many characteristics of the disease have been revealed [4]. Based on the epidemic situation, the government of each country continuously applies new measures to suppress the spreading.

In order to quantitatively evaluate and forecast the epidemic situation, a computer modeling is typically applied. For epidemic events, many conventional models are well reported in monographs [5],[6]. Typically, a simple compartmental model, which is so-called Susceptible-Infected-Recovered (SIR) model, is first considered. Extensions of the model in various aspects are possible with attempts to truly understand the nature of the epidemic in mind. In case of typical compartmental models, the number of populations is usually fixed. The changeability of this number will allow one to realistically trace the dynamics of disease spreading within this model.

In this work, we mainly consider the epidemic spreading of COVID-19 in Thailand. Attempts to improve the SIR model are made by fitting the reported data with various models. The changeable number of populations can improve the fitting while the abrupt change of the total populations can reflect the outbreak situation in Thailand at the beginning of March 2020. This study can aid the estimation of number of susceptible in Thailand. Global data of the cases in the world is considered and it shows that the epidemic has not reached the peak of the outbreak.

II. Epidemic Situation

Figure 1(a) shows the time evolutions of the cumulative numbers of confirmed, recovered, and death cases of COVID-19 cases in Thailand. They are defined as $N_C(t)$, $N_R(t)$, and $N_D(t)$, respectively. In Figure 1(a), the data is plotted for the overall period (22nd January – 21st April, 91 days) in log scale in order to show the data in broad view. The epidemic situation in Thailand is divided into two phases as shown in Figure 1(b). The Phase 1 is between 22nd January and 7th March (46 days) and the Phase 2 is between 7th March

The manuscript received May 2, 2020; revised May 24 and June 7, 2020; accepted June20, 2020. Date of publication June 30, 2020.

*Corresponding author: Assoc. Prof. Dr. Suwit Kiravittaya, Department of Electrical and Computer Engineering, Faculty of Engineering, Naresuan University, Ta-Pho, Muang, Phitsanulok 65000, Thailand (E-mail: suwitki@gmail.com)

– 21st April (46 days). This phase has started at the beginning of March (due to the infections in Soi Thonglor and Boxing

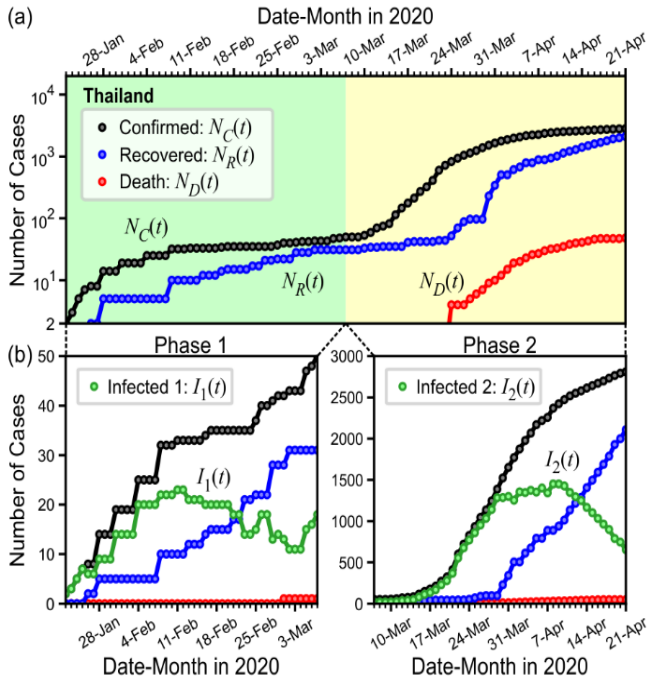

Fig. 1. Time evolution of the cumulative numbers of confirmed $N_C(t)$, recovered $N_R(t)$, and death $N_D(t)$ cases of COVID-19 cases in Thailand in (a) overall period (22nd January – 21st April, 91 days) in log scale, (b) phase 1 (22nd January – 7th March, 46 days) and phase 2 (7th March – 21st April, 46 days) in linear scale. In (b), the evolution of the numbers of infected $I_1(t)$ and $I_2(t)$ cases are plotted.

Stadium area) and has not yet ended (at the time of writing, 22nd April 2020) but it is approaching the end in May – June [7]. In Figure 1(b), the numbers of infected are defined as I_1(t) and I_2(t) and explained in the next sections. Similar trends of all quantities are observed in these two phases while the vertical scales are quite different. Due to the smaller numbers of cases in Phase 1, the existence of this infectious phase is not widely mentioned. However, the observed features can give a basic idea of this spreading.

III. Modified Compartmental Model

A conventional mathematical model for describing epidemic situations, which is so-called SIR model, is introduced first [5],[6]. It is a kind of compartmental model, where the population is divided into 3 groups. They are susceptible (S), infected (I) and recovered or removed (R). The numbers of members in each group are defined as $S(t)$, $I(t)$, and $R(t)$, respectively. This model can be written in differential equations as:

$$\frac{dS(t)}{dt} = -\beta \frac{S(t)\cdot I(t)}{N}, \tag{1.1}$$

$$\frac{dI(t)}{dt} = \beta \frac{S(t)\cdot I(t)}{N} - \gamma \cdot I(t), \tag{1.2}$$

and

$$\frac{dR(t)}{dt} = \gamma \cdot I(t). \tag{1.3}$$

The important model parameters are β and γ. The former is the mass-action term and it is the product of the average times of contact between susceptible and infected individual and the probability of the infection per contact event. The latter indicates the recovery rate, which is the rate that the number of infected changes to recovered or removed (death). Another parameter in this model is N. It is the total population that involved in the epidemic spreading. At the end of any epidemic spreading, most of the population becomes recovered. Normally, it is assumed to be 1 ($N = 1$) for the normalized population scheme. The numbers of S, I, and R are changed to population ratios in that case. Since the variation of population is considered in this work. We treat unnormalized N as a function of time (N becomes $N(t)$). Numerical method is applied to extract the solutions of Eqs. (1.1) – (1.3).

In order to solve the Eqs. (1.1) – (1.3), the initial condition must also be set. It is typically $S(0) = N_T - \delta$, $I(0) = \delta$ and $R(0) = 0$, where N_T is the initial total number of population and δ is the initial number of infected. In this work, the simulation study is done in Anaconda environment with Python language and Numpy and Scipy packages [8],[9].

The $I(t)$ and $R(t)$ can be extracted from the previously reported quantities ($N_C(t)$, $N_R(t)$ and $N_D(t)$ in Figure 1). According to the definition, the relations are:

$$R(t) = N_R(t) + N_D(t), \tag{2.1}$$

and

$$I(t) = N_C(t) - N_R(t) - N_D(t). \tag{2.2}$$

The evolution of $S(t)$ and total number of population $N(t)$ are typically not known but they can be estimated from the general evolution of the epidemic cases. Typically, $S(t \to \infty)$ is nearly zero while $R(t \to \infty) \approx N$ in the SIR model with a constant number of population N.

For the SIR model with changeable number of populations, we change N to $N(t)$ and consider its rate of change ($dN(t)/dt$). This is done based on the assumption that the involved population will change with the increasing social connection of the infected (who are not quarantined) and the applied measures (social distancing). Linear change of $N(t)$ is first considered due to its simplicity. Both increasing and decreasing of $N(t)$ can be treated by

$$\frac{dN(t)}{dt} = \alpha \cdot N_T \,, \tag{3}$$

where N_T is the initial total number of population and α is the normalized rate of change. The solution of Eq. (3) is simply a linear function:

$$N(t) = N_T \cdot (1 + \alpha \cdot t) \,. \tag{4}$$

This population change (Eq. (3)) is assumed to directly apply to the susceptible. The modified equations of the susceptible and infected (Eqs. (1.1) and (1.2)) are

$$\frac{dS(t)}{dt} = -\beta \frac{S(t) \cdot I(t)}{N(t)} + \alpha \cdot N_T \,, \tag{5.1}$$

and

$$\frac{dI(t)}{dt} = \beta \frac{S(t) \cdot I(t)}{N(t)} - \gamma \cdot I(t) \,. \tag{5.2}$$

The abrupt change of the population due to the occurred outbreak event (at the beginning of March) can be described by

$$\frac{dN(t)}{dt} = \Delta N \cdot \delta(t - t_c) \,, \tag{6}$$

where δ is the Dirac delta function and t_c is the critical time. This equation changes the number of populations from N_T to $N_T + \Delta N$ at the time t_c.

Figure 2 shows the selected simulation results for different models of $N(t)$. In all simulations, parameters are $N_T = 1{\cdot}10^5$, $I(0) = 100$, $S(0) = N_T - I(0)$, $R(0) = 0$, $\beta = 0.30$, and $\gamma = 0.05$. The simulation is done for 100 days with the time resolution dt = 0.01 day. Numerical error from the integration is checked by changing the resolution. No noticeable change is observed at smaller resolutions.

In Figure 2(a), the simulation results for a constant number of populations $N(t)$ ($N_T = 1{\cdot}10^5$) is presented as the reference case. In this case, the evolutions of $S(t)$, $I(t)$ and $R(t)$ are typical [5],[6]. The number of infected cases $I(t)$ increases to the maximum (~$5.4{\cdot}10^4$) at t ~35 days and then decreases slowly. In Figure 2(b), the value of α is set to +0.01. In this case, the maximum of the infected $I(t)$ ($7.1{\cdot}10^4$) is at t ~37 days. The number of infected does not go to zero at the end of the simulation (t = 100 days) since the number of susceptible still increases. This scenario might correspond to the real epidemic spreading event in many countries with an insufficient quarantine since the new infected can induce more susceptible in the SIR model.

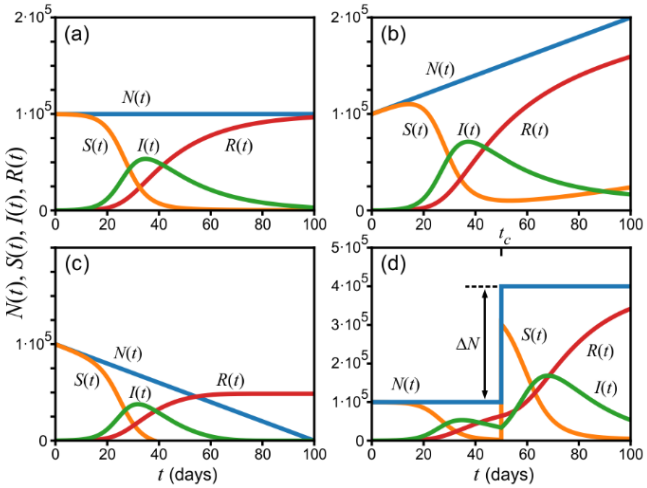

Fig. 2. Selected results from the models with changeable number of populations $N(t)$. (a) Constant $N(t)$, (b) linearly increasing $N(t)$, (c) linearly decreasing $N(t)$ and (d) step increasing $N(t)$.

In contrast to the SIR model with increasing population, the population reduction can also be simulated. A typical result is shown in Figure 2(c). The maximum number of infected ($3.8{\cdot}10^4$) is observed at t ~32 days. Both spreading time and the maximum number of infected are decreased with this model. It might look unrealistic at the first sight. But this model can improve the fits of the reported Thailand data as shown in Figure 3, This might correspond to the real situation as described below.

In order to explain the change of outbreak from phase 1 to phase 2, abrupt increase of the total population is assumed (Eq. (6)). Figure 2(d) shows the simulation result when the total numbers of population increases from $N_T = 1{\cdot}10^5$ to $4{\cdot}10^5$. This change induces the re-increase of the number of infected $I(t)$ and later the number of recovered $R(t)$. This result, which is one of the main contents of this work, can qualitatively fit the COVID-19 spreading scenario in Thailand. Since both $S(t)$ and N_T cannot be known beforehand, we can use this simulation to estimate them.

IV. Fitting of Two Infectious Period

According to the models with changeable number of populations shown in previous section, we can fit the reported data. The fit is done with the aid of *Scipy.optimize* package. The $N(t)$, $S(t)$, $I(t)$ and $R(t)$ in Eqs. (3), (5.1), (5.2) and (1.3) are solved simultaneously. The N_T is estimated and defined as N_{T1} for the phase 1 and N_{T2} for the phase 2. The results are fitted with observed $S(t)$, $I(t)$ and $R(t)$ with the least squares optimization scheme. The $I(0)$, β, γ, (and α) are the fitting parameters. Note that $S(t)$ is re-calculated after the estimation of N_T.

Fits with constant number of populations are show Figures 3(a) and 3(b). For phase 1, a constant population $N_{T1} = 50$ is assumed. After the fit, the obtained parameters are $I_1(0) = 5.145$, $\beta_1 = 0.1698$ and $\gamma_1 = 0.045355$. For phase 2, a constant

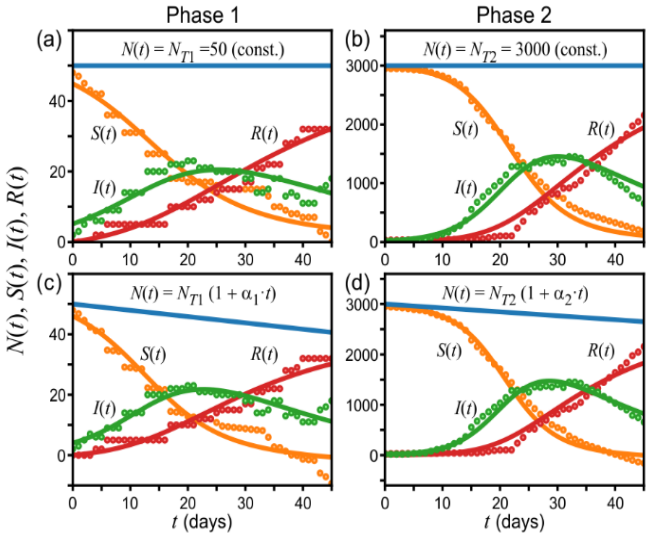

Fig. 3. Fits of Thailand data in phase 1 and phase 2. The fits were done with constant population model in (a) and (b) and linearly decreasing population model in (c) and (d). All data are simultaneously fitted with SIR model. The fitting parameters are $I(0)$, β, γ and α.

population N_{T2} = 3000 is assumed. After the fit, the obtained parameters are $I_2(0)$ = 19.95, β_2 = 0.2726 and γ_2 = 0.05359. The sums of squares of errors (SSE) in the fits of these two phases are 3.544×10^2 and 5.995×10^5, respectively. According to these results, the basic reproduction number R_0 of these two infectious events are β_1/γ_1 = 3.7 and β_2/γ_2 = 5.1. These values are higher than the initial reported values of ~2.2 [1] or 2.7 [10] for the epidemic spreading in China but it does agree with the recent report by Sanche *et al.* (4.7-6.6) on the re-examination of China data [11].

Improvement of the fitting results can be done with linearly decreasing population model. It can be clearly observed in Figures 3(c) and 3(d) that the fits of $S(t)$, $I(t)$ and $R(t)$ are simultaneously improved. According to the applied model and the data in phase 1, the obtained optimized parameters are $I_1(0)$ = 4.001, β_1 = 0.1987, γ_1 = 0.04309 and α_1 = -0.004159. For phase 2, the obtained parameters are $I_2(0)$ = 12.92, β_2 = 0.2974, γ_2 = 0.05123 and α_2 = -0.002592. The SSEs in the fits are 2.184×10^2 and 3.344×10^5 and the calculated R_0 are 4.61 and 5.81, respectively. The lowering of SSEs is the direct consequence of the considered model while the increased values of R_0 are the results from the decreasing population. Since the fits of the reported values are improved, we do believe that this scenario does truly reflect the epidemic event in Thailand. Since the news (information) about any new infected cases can spread faster than the physical spreading of virus, the initial susceptible might be removed from the population due to the increase of social distancing. It thus reduces the total number of populations.

It is noteworthy that negative values of $S(t)$ are observed at t > 40 days for both phases. This is unrealistic and implies that the nonlinear decreasing of the total population during the epidemic outbreak happens. However, modeling it without any further information is not possible.

Since the epidemic situations in two periods (2 phases) occurred with rather different measures, we do not make any attempts to fit both data with the same set of parameters. However, both phases can be connected by the abrupt increasing of the total populations as shown in Figure 2(d). Due to the property of the delta function, both total population $N(t)$ and susceptible $S(t)$ are discontinuous at the critical time t_c. According to the observed number of infected (Figure 1), we estimate this time is between 2nd and 4th of March 2020.

V. World Situation

According to the COVID-19 cases reported for all countries [3],[12], we can plot the epidemic situation in the similar way (Figure 1). Figure 4 shows the time evolution of the cumulative numbers of confirmed, recovered, and death cases of COVID-19 cases. In Figure 4(a), the data is plotted for the overall period (22nd January – 21st April, 91 days) in log scale. The world epidemic situation can also be divided into two phases as shown in Figure 4(b). Phase 1 is between January and the beginning of March.

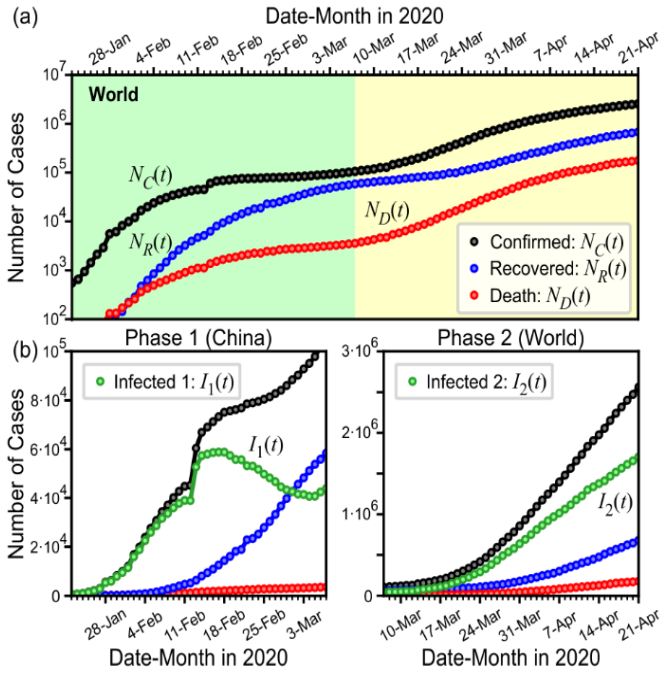

Fig. 4. Time evolution of the cumulative numbers of confirmed $N_C(t)$, recovered $N_R(t)$, and death $N_D(t)$ cases of COVID-19 Cases in the world in (a) overall period (22nd January – 21st April, 91 days) in log scale, (b) phase 1 (22nd January – 7th March) and phase 2 (7th March – 21st April) in linear scale. In phase 1, the epidemic mainly occurs in China and the outbreak starts at the end of February. In phase 2, the longer and larger outbreak has not been declined at the present time.

The exact dates are not important since the wide spreading is not occurred at the same date in each country. In phase 1, the spreading occurred mainly in China. The abrupt increase of

the confirmed case (on 12th February) is due to the data revision. We therefore do not quantitatively describe the data with our model. The epidemic outbreak in China seems to be ended since the number of infected $I_1(t)$ decreased (at the beginning of March). The total number of involved populations is ~83000. In phase 2, the epidemic spreading is over 180 countries and it does not have any sign of the end yet. Numbers of infected $I_2(t)$, recovered cases $N_R(t)$ and death cases $N_D(t)$ are still increasing. We therefore cannot confidently fit the reported results and extract the model parameters for this case.

VI. Conclusion

In conclusion, we present the COVID-19 data of Thailand and divide it into 2 phases. Modified compartmental model is presented. It relies on the combination of the conventional SIR model and the changeable number of populations. Fitting of the reported data suggests that the number of populations decrease with time while the connection between phase 1 and 2 can be explained by the abrupt increase of populations, which can be modeled by a delta function. World situation is briefly reported, and the described scenario of Thailand can be qualitatively applied to the world data. This work sheds light on the relationship between social impact and the control of the epidemic situation.

Note Added in Proof

Current data (29th May 2020) shows that the total infected population of Thailand is 3076. It is slightly above the initially estimated value of 3000. This might correspond to the infected group from aboard. The world pandemic outbreak has still no sign of the declination.

Acknowledgment

The author acknowledges the invitation of Assoc. Prof. Dr. Boonyang Plangklang for submitting this work. The discussion with Assistant Prof. Dr. Wanwisa Pansak is thankful. This work is supported by Faculty of Engineering, Naresuan University and Naresuan University via the Work-From-Home strategy.

References

[1] Q. Li, X. Guan, P. Wu, X. Wang, L. Zhou, Y. Tong, R. Ren, K. S. M. Leung, E. H. Y. Lau, J. Y. Wong, X. Xing, N. Xiang, Y. Wu, C. Li, Q. Chen, D. Li, T. Liu, J. Zhao, M. Li, W. Tu, C. Chen, L. Jin, R. Yang, Q. Wang, S. Zhou, R. Wang, H. Liu, Y. Luo, Y. Liu, G. Shao, H. Li, Z. Tao, Y. Yang, Z. Deng, B. Liu, Z. Ma, Y. Zhang, G. Shi, T. T. Y. Lam, J. T. K. Wu G. F. Gao, B. J. Cowling, B. Yang, G. M. Leung, and Z. Feng, "Early transmission dynamics in Wuhan, China, of novel coronavirus-infected pneumonia," *The New England Journal of Medicine*, vol. 382, pp. 1199-1207, 2020.

[2] https://en.wikipedia.org/wiki/2020_coronavirus_pandemic_in_Thailand

[3] https://www.worldometers.info/coronavirus/

[4] W. Guan, Z. Ni, Y. Hu, W. Liang, C. Ou, J. He, L. Liu, H. Shan, C. Lei, D. S. C. Hui, B. Du, L. Li, G. Zeng, K.-Y. Yuen, R. Chen, C. Tang, T. Wang, P. Chen, J. Xiang, S. Li, Jin-lin Wang, Z. Liang, Y. Peng, L. Wei, Y. Liu, Ya-hua Hu, P. Peng, Jian-ming Wang, J. Liu, Z. Chen, G. Li, Z. Zheng, S. Qiu, J. Luo, C. Ye, S. Zhu, and N. Zhong, "Clinical characteristics of coronavirus disease 2019 in China," *The New England Journal of Medicine*, February 28, 2020. DOI: 10.1056/NEJMoa2002032

[5] M. J. Keeling and P. Rohani, *Modeling Infectious Diseases in Humans and Animals*, Princeton University Press, New Jersey, 2008.

[6] E. Vynnycky and R. G. White, *An Introduction to Infectious Disease Modelling*, Oxford University Press, New York, 2010.

[7] S. Kiravittaya, "Fitting the evolution of COVID-19 cases of China and Thailand by applying piecewise linear approximation of compartmental model parameters," *Naresuan University Journal: Science and Technology*, vol. 28, pp. 91-101, 2020.

[8] R. Johansson, *Numerical Python - Scientific Computing and Data Science Applications with Numpy, Scipy, and Matplotlib*, Apress, New York, 2019.

[9] S. Linge and H. P. Langtangen, *Programming for Computations – Python*, 2nd Ed., Springer, Switzerland, 2020.

[10] J. T. Wu, K. Leung, and G. M. Leung, "Nowcasting and forecasting the potential domestic and international spread of the 2019-nCoV outbreak originating in Wuhan, China: a modelling study," *The Lancet*, vol. 395, pp. 689-697, 2020.

[11] S. Sanche, Y. T. Lin, C. Xu, E. Romero-Severson, N. Hengartner, and R. Ke, "The novel coronavirus, 2019-nCoV, is highly contagious and more infectious than initially estimated," https://doi.org/10.1101/2020.02.07.20021154

[12] https://github.com/CSSEGISandData/COVID-19

Preliminary Study of Flow Battery and Applications

Chairat Sornchai, Nirutti Nilkeaw and Boonyang Plangklang*

Department of Electrical Engineering, Faculty of Engineering,
Rajamangala University of Technology Thanyaburi, Pathumthani, Thailand

Abstract— This paper presents the study of Flow battery and applications. The Flow battery is divided into 2 categories. There are Redox Flow battery and hybrid Flow battery that used for each application. The flow battery contains the chemical solution in the liquid state which used motor pumping to circulate the energy for exchanging at the membrane separator. The charging of the Flow battery is basically as Lead-Acid battery. Many advantages of the Flow battery and application of the energy storage system and it can be used for storage the huge energy with high efficiency. However, the Flow battery is needed to study in a technical detail and develop in optimal condition from each application in near future.

Keywords—flow battery, Redox flow battery, hybrid flow battery.

I. INTRODUCTION

Recently, modern loads are increased to the grid and high impact on the energy consumption from the grid. Energy demand is a key performance of the energy response and the stability margin of the network. The variation of the energy demand from each customer needs to manage and provide in optimal condition. The role of the energy sources is becoming a point to solve and prepare for supporting the load variation. Thus, renewable energy sources (REs) are selected to support the grid in a backup condition by an energy control provider. The REs are generating from the natural and environmental factor and instability from the seasonal. So, the REs needed to store and backup the energy generated for continuing electric generation.

Energy storage system (ESS) had used to store the surplus energy from the main energy sources and regenerate energy to the grid in bi-direction power flow. Application on peak shaving and peak demand reduced are interesting to adapt the ESS [1]. The ESS technology is rapidly developing efficiency in a strategy and technical term. Many researchers are present the methodology to study and apply in a commercial sector and extend sizing of a capacity with area used. Traditional ESS types are presented in a mechanic energized as fly wheeling techniques and hydraulic storage as presented in [2] which used large scale of area per energy storage capacity. Many types of the ESS are provided and support by defined from the problems of the electrical power system. A battery is a majorly part of the ESS by using electrochemical techniques. Therefore, this ESS type relates the types of the battery. The battery is used for storing the electrical energy by using charge and discharge process. Lead-Acid (LA) battery type is a traditional of the battery which widely uses and adapts to the ESS. The effect of the charging cycle and charging method relates to the shortage of the lifetime. So, many types of the battery are developed by researchers which subject to extend the lifetime and increase the efficiency. Flow battery is one type of a modern battery technology and popularly develops for storing the energy [3].

This paper is organized as follows. First, the basic principle and characteristics of Flow battery is explained. Then, the basic of Flow battery characteristic and flow battery performance are proposed in section III. The advantage-disadvantage, application and benefits of Flow battery are presented in section IV and V, respectively. Finally, the conclusions and discussion work are presented in section VI.

II. PRINCIPLES AND CHARACTERISTICS OF FLOW BATTERY

Flow Battery works with the flow of electrolyte solution which is the part that stores energy through electrochemical cells. The electrolyte solution consists of one element or compound or more that has electrochemical characteristics. The electrochemical cell which consists of a cathode and anode separated by

The manuscript received April 29, 2020; revised May 27, 2020; accepted June 20, 2020. Date of publication June 30, 2020.

*Corresponding author: Assoc. Prof. Dr. Boonyang Plangklang, Dept.of Electrical Engineering, Faculty of Engineering,Rajamangala University of Technology Thanyaburi, Pathumthani, Thailand 12110
(E-mail: boonyang.p@en.rmutt.ac.th)

a membrane is used to convert chemical energy into electrical energy. The electrolyte solutions are located in the tanks outside the cell and pumped into the cell for reaction. The reaction will be reversible and related to the process of charging and discharging as shown in Figure 1. Therefore, the power depends on the number and the area of cells while the energy depends on the concentration and amount of the electrolyte solution.

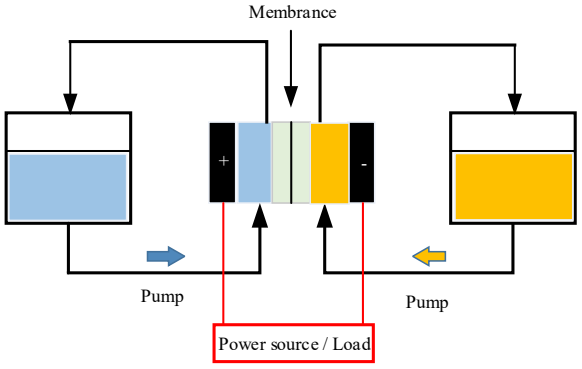

Fig.1 Flow chart of the battery that has the flow of energy storage (Flow Battery) [3]

Flow Battery can be divided into 2 large groups, Redox Flow Battery and Hybrid Flow Battery. Each group can be presented in details as follows.

Redox Flow Battery

Redox stands for Reduction-Oxidation. It is an electrochemical reaction that provides and receives electrons between substances. It has an electron transfer in which the oxidation reaction, molecules or atoms lose electrons from orbit to molecules that act as electron receptors Oxidation and reduction reactions occur in pairs. Substances that act as electrons "electrochemistry" are the relationship between chemical reactions and electrical energy. In which the chemical process occurs when electrons are transferred chemical reactions cause electrical energy. On the other hand, electrical energy can also cause chemical reactions. Examples of batteries of this group are vanadium redox battery (VRB) and Polysulfide Bromide Battery, etc.

A.1 Vanadium Redox Battery (VRB)

VRB stores energy by using an electrolyte solution which is a vanadium solution in sulfuric acid. The storage tank of the anode is a vanadium solution with an oxidation number of +2 and +3, while the cathode is a vanadium solution with an oxidation number of +4 and +5, as in Figure 2[4].

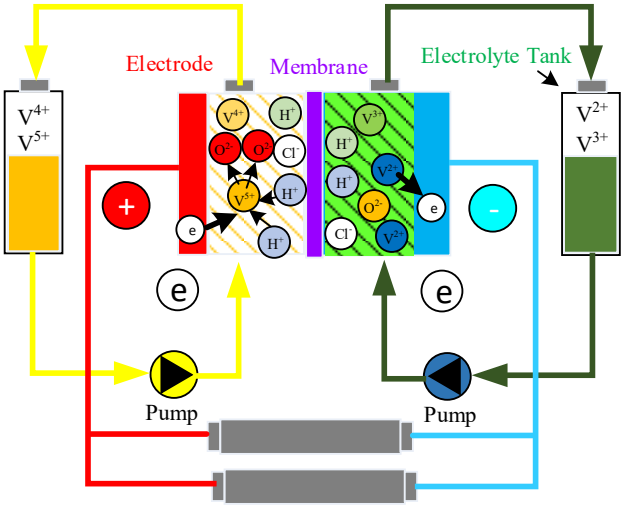

Fig.2 Flow chart of Vanadium Flow Battery [5]

Within the cells container, both electrolytes are separated by a proton exchange membrane. Although both electrolytes are the same substance, vanadium but the positive half-cell contains VO_2+ and VO^{2+} ions, while the negative half-cell contains V^{2+} and V^{3+} ions. There are many ways to prepare an electrolyte solution including dissolving vanadium pentoxide (V_2O_5) in sulfuric acid by the electricity. This solution is highly acidic. During the flow process, both half-cell solutions are contained in a large storage tank and are simultaneous pumped through the cells to generate electricity. While charging the flow battery, VO_2+ which in the positive half-cell is changed to VO^{2+} when the electrons (e^-) fall out of the anode and run into the negative half-cell and change V^{3+} to V^{2+}. On the other hand, during discharged, the process will be reversed which causes the open circuit voltage to be 1.41V.

A.2 Polysulfide bromide batteries (Polysulphide Bromide Battery; PSB)

In PSB-type battery, there is a chemical reversal reaction between two salt solutions, sodium bromide (NaBr) and sodium polysulfide (Na_2S_4). The two parts electrolyte solution is separated by a membrane called polymer which allows sodium ions to pass through. The electric potential of the cell is 1.5V and the overall efficiency is about 75 percent as shown in Figure 3.

Hybrid Flow Battery

Hybrid Flow batteries use electrochemical components consisting of one battery electrode and one fuel cell electrode. The use of 2 different types of electrolyte solutions can be allowed the exchange of electrons through the membrane for power generating. Examples of batteries of this group are zinc bromine batteries. (Zinc-Bromine: ZnBr) and zinc cerium batteries (Zinc-Cerium) [6].

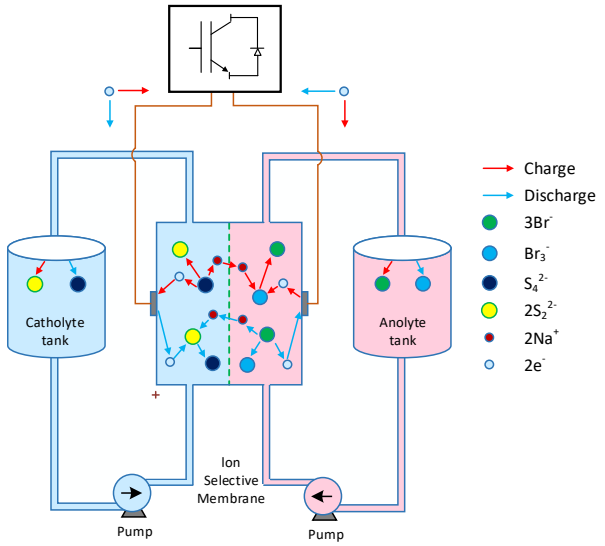

Fig.3 Flow chart of Polysulphide Bromide Battery [7]

B.1 Zinc Bromine Battery (ZnBr)

In each cell of ZnBr, there are 2 different electrolyte solutions flowing through carbon-plastic electrodes. Both electrodes are separated using a small porous polyolefin membrane. During discharging, Zn and Br combine to form zinc bromide. Increasing of the density of Zn^{2+} and Br^- in the electrolyte solution as shown in Figure 4 [8].

During the electrolyte collection, zinc is stored as a thin film on one side of the electrode. While bromine will react with organic amine, which is sticky bromine oil deposited into the bottom of the electrolyte tank. Dilute the electrolyte on the other side of the membrane. The electric potential of the cell is approximately 1.8 volts. The overall efficiency is around 75 percent.

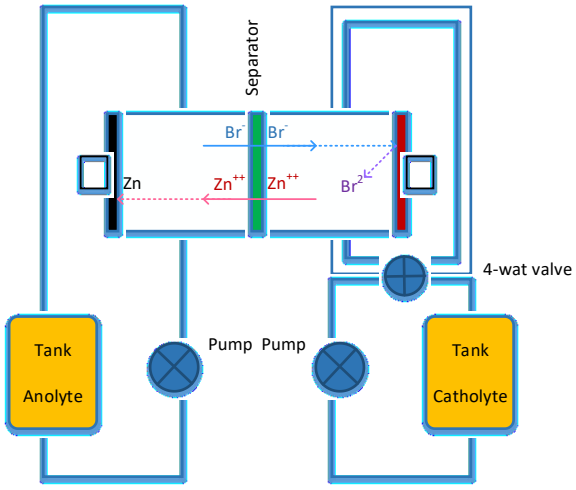

Fig.4 Flow chart of Zinc Bromine Battery [9]

2.2 Cerium zinc battery (Zinc-Cerium)

Zinc-Cerium uses two electrolytes, namely Negative Zinc and Positive Cerium, to conduct an electrochemical exchange of electrons that are separated by Nafion (DuPont) Cation Exchange Membrane, resulting in the reaction of Ce (III)/Ce(IV) compounds at the positive electrode and Zn (II)/Zn at the negative electrode. In general, the electric potential of the chemical reaction from zinc and cerium redox has a high standard causes the voltage of the open circuit cell up to 2.43V. [10].

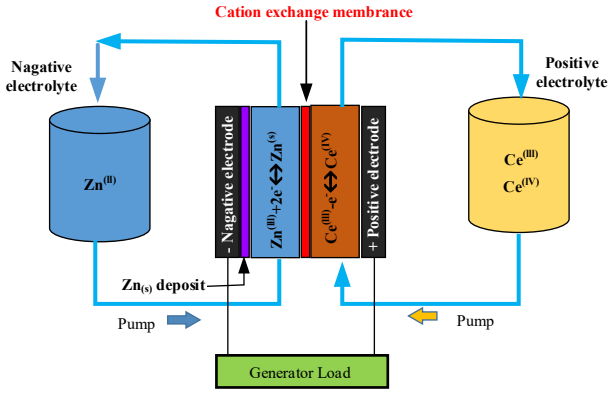

Fig.5 Zinc-Cerium Battery flow chart [11]

However, a wide range of chemistries have been tried for flow batteries. There are different of maximum cell voltage (V), average electrode power density (W/m2), average fluid energy density (W·h/kg or W·h/L), and cycles.

III. The Basic of Flow Battery Characteristic and Flow Battery Performance

The power capacity of the battery is dependent upon the number of cells in the stack. An average discharge voltage was determined by taking the average of all voltages through the discharge cycle and then used to determine the number of cells needed. Figure 5 shows how the voltage changes as the battery discharges in one cell, which means that the power output also decreases because the current is constant and power = V * I [12].

The performance of Flow Battery can be measured with three efficiencies: current efficiency, voltage efficiency, and energy efficiency. The current efficiency (CE, Columbic efficiency) is defined as the ratio of the amount of usable charge to the stored charge amount, that is, the discharge capacity divided by the charge capacity.

CE is a measure of the storage capacity loss during charge-discharge process. The capacity loss is mainly caused by the crossover of the electrolyte ions through the membrane. The mixed active materials result in a capacity imbalance between the anode and cathode electrolytes and an irreversible capacity loss.

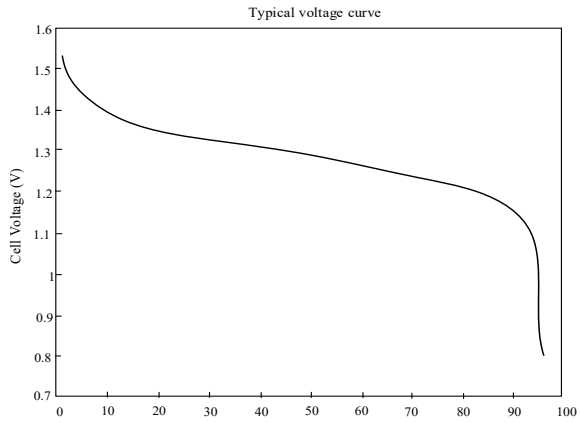

Fig.6 Flow Battery voltage curve [13]

IV. Advantages - Disadvantages of Flow Battery

Flow battery is useful to adapt in the storage system. However, it may have advantage in some application can be explained as follows.

1. Flow battery can be designed separately between electric power and energy. In which the number of electrochemical cells determines the electric power and the amount of electrolyte determines the amount of energy.

2. The self-releasing energy. (Self-discharge) is small, has a fast response time with high efficiency.

3. Completely discharging able to store energy longer than other batteries.

4. Can quickly re-charge the battery many times. In an unlimited capacity since energy is collected through a liquid medium, an electrolyte solution.

The disadvantages of Flow Battery can be described as.

1. Low energy density (below 15 kWh /m3)

2. Most electrolyte solutions have an acidity value. Causing environmental toxicity

3. Product Price, operation and maintenance cost is quite high since the system has many components, including pumping systems, flow control systems and ion exchange membrane (ion-exchange membrane)

4. There is a usage limitation caused by the flow of electrolytes makes it difficult for use in mobile applications such as use in cars.

V. Application and Benefits

The main feature of Flow Battery is that it can charge new energy. Has a large capacity Has the power and the level of independent work force (Can be adjusted up and down easily) in a large tank separate from the battery Which is different from conventional batteries in which the electrode is solid and contained in the battery Resulting in limited size and energy. The advantage of this battery is that it can be used with large systems more easily than other types of batteries. By expanding the size of the tank and increasing the amount of electrolyte solution Therefore, this type of battery can be used for large-scale energy storage applications. Such as backing up energy from wind or solar energy or from a large generator providing the ability to produce electricity efficiently increasing efficiency in storing and distributing electricity more quickly makes it able to cope with the demand for electrical power in the future. Flow Battery research and development Flow Battery development to focus on increasing efficiency in energy density more stable electrolyte solution and reduced system installation costs to be applied to reserve power with a larger system. There are several methods of development that can be done as follows [14]

1. Changing the material used for an electrode making.

Anode and Cathode in Flow Battery are generally materials that have basic carbon components. Like other battery technologies, electrodes are an extremely important component of battery performance. To increase the electrochemical reaction of the electrode, the electrode material should have low resistance and a large specific area. Therefore, changing the material of the electrode used for the electrode making will also change the performance of the battery. For example, the use of graphite-containing materials will make the ability to turn (reversibility) and higher current density.

Likewise, increasing the surface area or the size of the electrode will also increase the amount of electrical energy. If the battery is needed to remain the same size, the development of the surface area of the electrode by coating with a substance containing particles that are numerous nanometers may perform. These will create a tremendous amount of surface area resulting in an increase in the amount of electrical energy.

2. Changing the electrolyte solution

Changing the electrolyte solution in the Flow Battery leads to better balance which can improve the performance of the system such as increase the ability to store more power in the battery as well, helps to work at higher temperatures, and also resulting in a smaller size of the electrolyte tank while maintaining the same electrical capacity. In general, sulfuric acid, which is used as a solution in the Flow Battery, works well in temperatures from 10 °C to 40 °C. The ions in the sulfuric acid crystallize which will cause the battery to heat up. Therefore, the installation of air conditioning or cold water to control the temperature of the battery is needed. These will cause more energy loss and also increases the operating cost of the battery. The development of an electrolyte solution can work at a wider temperature and will be able to reduce the cost of installing the cooling system with the battery performance remaining the same or improving.

3. Changing the membrane

Normally, the tanks used to contain the electrolyte solution are separated by ion exchange membranes. When charging the battery, there will cause metal ions to oxidize or decrease due to reactions that convert chemical energy into electrical energy. The ion exchange membrane protects and stores the ions inside the tank. While allowing protons to pass by but the membrane in general perfluorinated Polymers, such as Nafion, allow some of the ions to pass through and are expensive, so batteries using this type of membrane will have limitations in commercial production. Charging the membrane made from Polyacrylonitrile, The pores of this type of membrane allow for better control of the ion

passing from one side of the battery to the other during charging and discharging which is to improve the efficiency of the battery and still have a cheaper price.

In addition, the development of materials used as membranes with a greater number of pores, but reducing the size of the pores to be as small as nanometer which found that this type of membrane allows more protons to pass through.

VI. CONCLUSIONS

Flow battery technology is a technology for storing electrical energy using electrochemical cells with unique characteristics compared to conventional batteries. Such as the ability to separate maximum energy from a given energy capacity and with more design flexibility, resulting in a high efficiency Flow Battery able to supply electricity quickly Has a high voltage circuit can be developed for use as a large energy storage system such as electric power from renewable energy Whether from solar energy, wind energy, bio-gas or other biomass energy as well. However, there are still some limitations in using it, especially in applications that are moving, such as cars, etc. Therefore, the study to develop Flow battery to be able to use efficiently including the production widely used in commercial is so important.

REFERENCES

[1] L. A. Wong, V. K. Ramachandaramurthy, P. Taylor, J. B. Ekanayake, S. L. Walker, and S. Padmanaban, "Review on the optimal placement, sizing and control of an energy storage system in the distribution network," *Journal of Energy Storage,* vol. 21, pp. 489-504, 2019/02/01/ 2019.

[2] Haoran Zhao, Qiuwei Wu, Shuju Hu, Honghua Xu, and Claus Nygaard Rasmussen, "Review of energy storage system for wind power integration support," *Applied Energy*, vol. 137, pp. 545-553, 2015/01/01/ 2015.

[3] Adam Z. Weber, Matthew M. Mench, Jeremy P. Meyers, Philip N. Ross, Jeffrey T. Gostick, and Qinghua Liu, "Redox flow batteries: a review," *Journal of Applied Electrochemistry*, vol. 41, no. 10, p. 1137, 2011/09/02 2011.

[4] Wilson, I, A, G., McGregor, P, G. and Hall, P, J., (2010) Energy storage in the UK electrical network: Estimation of the scale and review of technology options. Energy policy, 38 : 4099-4106.

[5] Nair, N, C. and Garimella, N., (2010) Battery energy storage systems : Assessment for small-scale renewable energy integration. Energy and building, 42 : 2124-2130.

[6] Beaudin, M., Zareipour, H., Achellenberglabe, A. and Rosehart, W., (2010) Energy storage for mitigating the variability of renewable electricity sources: An updated review. Energy for Sustainable Development, 14 : 302–314.

[7] Ibrahim, H., Ilinca, A. and Perron, J., (2008) Energy storage systems-Characteristics and comparisons. Renewable and sustainable energy reviews, 12 : 1221-1250.

[8] Baker, J., (2008) New technology and possible advances in Energy storage. Energy Policy, 36 : 4386-4373.

[9] Hadjipaschalis, I., Poullikkas, A. and Efthimiou, V., (2009) Overview of current and future energy storage technologies for electric power applications. Renewable and sustainable energy reviews, 13 : 1513-1522.

[10] Peng, B. and Chen, J., (2009) Functional materials with highefficiency energy storage and conversion for batteries and fuel cells. Coordination chemistry reviews, 253 : 2805-2813.

[11] Joerissen, L., Garche, J., Fabjan, C. and Tomazic, G., (2004) Possible use of vanadium redox-flow batteries for energy storage in small grids and stand-alone photovoltaic systems. Journal of power sources, 127:98-104.

[12] Mohamed, M.R., Sharkh, S.M., and Walsh, F.C. Redox Flow Batteries for Hybrid Electric Vehicles: Progress and Challenges. Vehicle Power and Propulsion Conference, 2009. VPPC'09. IEEE. 2009: p. 551-557, DOI.

[13] Wagner, R. Large lead/acid batteries for frequency regulation, load levelling and solar power applications. Journal of Power Sources. 1997. 67(1–2): p. 163-172, DOI: http://dx.doi.org/10.1016/S0378-7753(97)02509-3. 36

[14] VRB Power Systems Inc. The VRB Energy Storage System (VRB-ESS TM) An Introduction to Wind & the Integration of a VRB-ESS (last acessed in 05/12/2012). 2007; Available from: http://www.vrbpower.com/publications/casestudies.html.

[15] REDT -Renewable Energy Dynamics Technology Ltd. (last acessed in 12/06/2013). Available from: IEEE. 2009: p. 551-557, DOI.

Effect of Oxygen-free Ice Produced by Fine Bubble Technology on Microbial Contamination and Sensory Preference of Asian Sea Bass (*Lates calcarifer*) Preservation

Boontarika Thongdonphum*, W. Pivsa-Art, S. Pivsa-Art, S. Pavasupree, K. Yoshikawa
Rajamangala University of Technology Thanyaburi,
Pathum Thani, Thailand

Abstract: Effects of oxygen-free ultra-fine bubbles ice on the preservation of Asian sea bass (*Lates calcarifer*) was studied. This species is significant aquaculture economic values in Thailand. To assess the applicability of ultra-fine bubbles technology for preservation, three types of preservation were tested using different types; (1) keep in normal ice (Treatment 1 or T1), 2) keep fish in oxygen-free ice; OFI (T2), and 3) freeze (T3). Twelve days, physical sensory preference scores of the Asian sea bass were evaluated for the three treatments. The oxygen free ice has a positively impact between Day 4 and Day 8 on the physical quality and sensory preference of Asian sea bass. The finding showed the OFI is found to be substantially successful in maintaining Asian sea bass freshness. However, the results revealed that the Asian sea bass retained in regular ice during the experiment displayed a dramatic shift in its color.

Keywords*—Oxygen-free ultra-fine bubbles ice, Preservation, *Lates calcarifer

I. INTRODUCTION

Seafood is one of the major natural economic products and a favorite diet of Thailand [1]. Asian sea bass (*Lates calcarifer*) is an extremely good source of protein economically importance worldwide, yet very low in fat and calories, making them a very healthy food choice. Formaldehyde or formalin is commonly used as tissue preservatives. Many fish sellers spray or dip fish with formalin-treated water to keep seafood products looking fresh for longer period of time, where this chemical puts public health at risk [2].

The presence of formaldehyde in fresh seafood has been notice in the fresh market, flea market and field far from the coastal region [3]. Cooling, packaging in modified atmosphere preserves the fresh fish products. Of these products, the microflora is often complex. Much of the spoilage is from microbial action [4]. Aerobic bacteria that decompose fish protein using dissolved oxygen (DO) in water initiate degradation mechanisms for maintaining fish freshness in water. Oxygen-free water can significantly suppress bacterial activity and increase the time need to maintained freshness. This approach has the benefit that it is absolutely free, without any chemical additives.

Nowadays, micro/nano bubble (MNB) technologies are evolving rapidly in various field [5], especially in Japan. Micro/Nano-bubbles technology based on realistic bio-applications, the production of biological treatment at the cell-level [6]. Fine bubbles (FB) technology, bubbles consisting of micro bubbles (1μm<MB<100μm dia.), and ultra-fine bubbles (UFB<1μm dia.), is now rapidly emerging as an innovative technology in different fields [5].

Thongdonphum et al. [7] stated that between Day 4 and Day 8 the oxygen free water and ice positively affected the physical quality and sensory preference of Threadfin bream. The mechanism for preserving fish freshness is as follows; as fish degradation in water is caused by aerobic bacteria which decompose fish protein using dissolved oxygen in the water, oxygen-free water can greatly suppress the activity of such bacteria, resulting in long-term preservation of fish freshness.

The method's greatest benefit is absolutely free, without any chemicals. Yoshikawa and Thonglek [5] reported that ultra-fine bubbles of oxygen were measured and found to remain longer under atmosphere conditions, for as long as one month. It has also been proved that free radicals are generated during the microbubble collapse, which can very strongly kill bacteria [8, 9]. For OFW, on the other hand, to prevent oxygen re-dissolution into water, OFW must be kept free of air contact [7].

In this analysis, oxygen-free ice produced by fine bubble technology was applied to preserve Asian sea bass. To compare with traditional, the microbial count and spoilage on fish skin were tested.

Manuscript received June 14, 2020; revised June 26, 2020; accepted June 29, 2020; Date of publication June 30, 2020.

*Corresponding author: Asst. Prof. Dr. Boontarika Thongdonphum is with Faculty of Agricultural Technology, Rajamangala University of Technology Thanyaburi, Thanyaburi District, Pathum Thani, 12130, Thailand (Email: Boontarika@rmutt.ac.th).

II. METHODOLOGY

A. Fish Source

Asian sea bass was harvested from the fish farm, Chachoengsao Province, Thailand, and transported to the laboratory within around 3 hours. The Asian sea bass had a total weight of approximately 700 g/individual per treatment and was tested at normal temperature in each treatments and tested for 12 days in plastic bags in the iced storage box in the room.

B. Experimental design

All experiments followed a completely randomized design (CRD) consisting of three treatments as follows: fish preserved in standard tap water ice (NI, Treatment 1 or T1), fish in oxygen-free ice (OFI) (T2). Fish samples T1 and T2 were placed in ice storage boxes containing ice layers using a 1:2 (w/w) of fish/ice ratio, while T3 was designed to test the air freezing still.

Fish have been divided into 27 group samples. Then, nine group samples were divided into three batches. Evaluation of physical parameters for every batch was recorded for a total of 12 days every 4 days. They were not returned to the experiment after the samples were analyzed in each group.

Fish samples weighting 700 g per group were individually packed in polyethylene bags (PE) and then divided into groups for sensory tests in 12 days. Fish were prepared according to the above experimental design, and kept at less than 5 ºC in iced storage boxes.

Ice was frozen at twice the weight of the fish in the storage boxes and refilled every day to preserve the consistency of the fish [10] and to avoid changes in various chemical and physical factors after processing and storage [11]. The ratio of fish samples/ice was held at 1:2 and regular replacement of the melted ice in the storage boxes [12] was undertaken. Evaluation of microbial change during the 12-day period was conducted every 4 days.

C. Oxygen-free water

An economical but high performance RMUTT-MNB generator was developed at RMUTT to generate N_2-FB, based on the pressurized dissolved gas method (Fig. 1) for basic research. A generator of RMUTT-MNB can generate many tens of thousands/mL of microbubbles (MB), and ultra-fine bubbles (UFB) up to 10^6 nitrogen bubbles/mL, (Fig. 2), measured with Malvern Panalytical NanoSight NS300.

Oxygen-free water (OFW) was made from distilled water. Prior to production, a once-through cleaning of all the generator channels was performed using distilled water for 20 min with a flow rate of 1 L/min. The MNB generator had dead space of about 0.4 L.

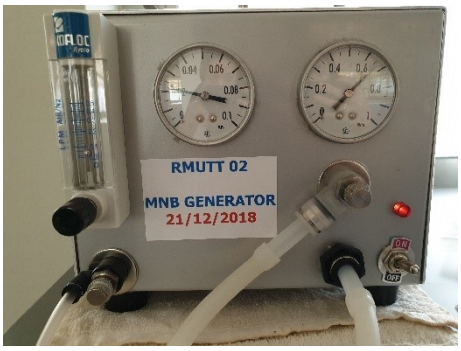

Fig. 1. RMUTT-MNB generator developed for basic research at RMUTT.

Nitrogen FB was injected and recirculated for 15 min with nitrogen gas flow rate of 0.05 L/m by the MNB generator to 10 L water in the plastic bottle, resulting in DO of approximately 0.18 mg/L and average OFW size of 179.3 nm±134.5 nm (Fig. 2).

OFW was produced by an in-house micro/nano bubble generator at RMUTT, packed in 20L plastic hard bottles. The OFW was contained in plastic bags to produce oxygen-free ice at -20 ºC. The OFW was used immediately to preserve fish without any delay, to keep OFW as real OFW and to reduce the contact time with air.

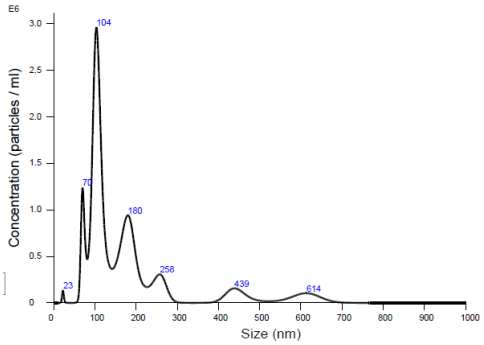

Fig. 2. Size measurement of ultra-fine nitrogen bubbles in oxygen-free water and concentration (bubbles/mL) produced by an RMUTT-MNB generator.

III. RESULTS

Fish preservation

Fish samples were packed in plastic bags at approximately 700 g weight in each 12-day treatment at RMUTT. Table 1 shows results. Fish preserved in oxygen-free ice (OFI) were found to be in excellent condition after 4 days and comparable to those brought from the market, while fish in normal ice (T1) showed a shift in light color and smell as opposed to live fish skin.

The results on Day 4 showed the highest overall parameter score was freezing, following by OFI and NI, respectively, while the results on Day 8 showed a similar pattern compared to Day 4. The overall results in the fish preservation test had the high score in sequence, freezing, OFI, and NI, respectively, when considered in each parameter shown in Table 1.

TABLE I
PHYSICAL PREFERENCE TEST SCORES OF FISH PRESERVATION FOR THE THREE TREATMENTS

Day	Treatment	Physical preference scores				
		Eyes	Gill	Skin	Odor	Texture
0	T1	4.9±0.3^{a}	5.0±0.0^{a}	5.0±0.0^{a}	4.4±0.5^{a}	5.0±0.0^{a}
	T2	5.0±0.0^{a}	4.7±0.5^{a}	5.0±0.0^{a}	4.5±0.5^{a}	5.0±0.0^{a}
	T3	5.0±0.3^{a}	5.0±0.0^{a}	4.9±0.3^{a}	4.6±0.5^{a}	4.9±0.3^{a}
4	T1	3.8±0.2^{a}	3.5±0.2^{a}	3.8±0.5^{a}	3.5±0.6^{a}	3.3±0.7^{a}
	T2	3.5±0.6^{a}	3.8±0.6^{b}	3.9±0.8^{a}	3.5±0.6^{a}	3.4±0.7^{a}
	T3	4.7±0.3^{b}	4.1±0.3^{c}	4.2±0.6^{a}	3.7±0.5^{a}	3.6±0.5^{a}
8	T1	3.3±0.5^{a}	3.1±0.6^{a}	3.8±0.5^{a}	3.5±0.6^{a}	3.3±0.7^{a}
	T2	3.3±1.0^{a}	3.1±1.1^{a}	3.9±0.8^{a}	3.5±0.6^{a}	3.4±0.7^{a}
	T3	4.3±0.5^{b}	4.0±0.6^{a}	4.2±0.6^{a}	3.7±0.5^{a}	3.6±0.5^{a}
12	T1	2.2±0.9^{a}	1.8±0.5^{a}	2.1±0.4^{a}	2.3±0.7^{a}	1.9± 04^{a}
	T2	2.3±0.7^{a}	2.3±0.5^{a}	2.2±0.5^{a}	2.9±0.5^{a}	2.5±0.5^{a}
	T3	3.9±0.4^{b}	3.9±0.5^{b}	3.9±0.3^{b}	4.0±0.0^{b}	4.0±0.1^{b}

Note: The values in the same column with different superscript letters are significantly different ($p \leq 0.05$).

Evaluation of Bacteria

Results of microbial assessment on fish skin in each treatment are shown in Table 2. Measurements of changes in microbial quality were taken every 4 days for a total period of 12 days. Observations of total bacteria on fish skin were compared on the 1st, 4th, 8th and 12th day. The overall findings showed that freezing (T3) obtained the lowest of total bacteria followed respectively by OFI (T2) and NI (T1).

Day 4 test revealed that freezing produced the lowest total number of bacteria followed by OFI and NI, respectively. Results at the end of the experiments, exhibited freezing as the most effective for fish preservation, while oxygen-free ice made from RMUTT-MNB had a positive influence on the number of total bacteria.

TABLE II
EVALUATION OF TOTAL BACTERIA (CFU/ML) ON SKIN OF FISH PRESERVATION FOR THE THREE TREATMENTS

Treatment	Day			
	0 ($\times 10^5$)	4 ($\times 10^5$)	8 ($\times 10^5$)	12 ($\times 10^5$)
T1	0.73±0.00^{a}	0.64±0.46^{a}	8.38±0.96^{b}	21.88±1.63^{c}
T2	0.54±0.00^{a}	0.94±1.28^{a}	6.33±2.64^{b}	13.52±0.05^{b}
T3	0.25±0.00^{a}	0.17±0.00^{a}	2.88±0.12^{a}	6.51±4.39^{a}

Note: The values in the same column with different superscript letters are significantly different ($p \leq 0.05$).

The number of total bacteria in meat (Table 3) differentiated significantly between the three experimental groups when compared in each treatment, particularly on Day 8 and 12. In comparison, the total bacteria values in meat displayed the lower average bacteria values on the skin relative to the total bacteria.

Overall finding showed that freezing (T3) also hit the lowest total bacteria followed respectively by OFI (T2) and NI (T1). TABLE II

EVALUATION OF TOTAL BACTERIA (CFU/ML) IN MEAT OF FISH PRESERVATION FOR THE THREE TREATMENTS

Treatment	Day			
	0 ($\times 10^5$)	4 ($\times 10^5$)	8 ($\times 10^5$)	12 ($\times 10^5$)
T1	0.47±0.00^{a}	1.45±1.23^{a}	9.68±0.97^{c}	18.76±23.00^{c}
T2	0.16±0.00^{a}	0.32±0.07^{a}	2.38±1.02^{b}	10.02±0.29^{b}
T3	0.15±0.00^{a}	0.11±0.17^{a}	0.24±0.10^{a}	5.83±2.53^{a}

Note: The values in the same column with different superscript letters are significantly different ($p \leq 0.05$).

IV. DISCUSSION

Reasons for declining fish quality leading to spoilage need to be carefully evaluated. Depending on the individual the time of pre-rigor mortis and rigor mortis varies. It also depends on a variety of factors, such as temperature, handling, size, physical condition, bio-chemical reactions and microorganism activities of the fishes [12].

In the detailed studies of the Food and Agriculture Organization (FAO) on the use of ice in fish preservation, when ice is used to lower temperature to about 0 ^{o}C, the growth of spoilage and pathogenic micro-organisms are reduced [13], as well as the rate of enzymatic reactions, in particular those associated with early rigor mortis period.

Gradual degradation of color, texture and taste during extended of storage frozen shrimps becomes apparent organoleptically [14]. Products stored in the upper shelves of horizontal freezers were frequently exposed to temperatures close to 10 ^{o}C, while recommended storage temperatures were only reported on the lower shelves. Deviations in the temperature of domestic storage were even more pronounced, with reported temperatures in some cases as high as 5 ^{o}C.

Oxygen is needed for the growth of aerobic bacteria, but the flushing of nitrogen gas can be deleterious to bacteria [15, 16]. Bacteriological analysis is used to determine the potential existence of microorganisms of public health importance and to give an indication of the fish's hygienic condition [17].

Thus, in our experiments, nitrogen bubbling in a form of ultra-fine bubbles could penetrated fish meat through skin and visceral, preventing oxidation of oil and fat content, as well as aerobic bacteria's activity and growth. In such condition freshness is kept with good taste for at least 8 days [18].

V. CONCLUSION

Results revealed that the oxygen-free ice also had positive effects for 4 days on physical quality and sensory preference of fish freshness. Experiments also demonstrated the applicability of ultra-fine bubble technology as an option for enhancing fish product shelf life.

ACKNOWLEDGMENT

The authors would like to extend deep gratitude and deep appreciation to the Research Institute and Faculty of Agricultural Technology, Rajamangala University of Technology Thanyaburi (RMUTT) for all the support given during this study.

REFERENCES

[1] S. Osiri, "Sea food safety situation in the East," *Thailand Journal of Health Promotion and Environment Health*, pp. 74-86, 2009. Available: http://digi.library.tu.ac.th/index/0125/32-4-Oct-Dec-2552/08PAGE74-PAGE86.pdf

[2] N. Jaman, Md. S. Hoque, S. C. Chakraborty, Md. E. Hoq and H. P. Seal, "Determination of formaldehyde content by spectrophotometric method in some fresh water and marine fishes of Bangladesh," *International Journal of Fisheries and Aquatic Studies*, Vol. 2, No. 6, pp. 94-98, 2015.

[3] V. Somjit, K. Yooyen and C. Kwannak, "Survey of formalin contamination in popular seafood from fresh market and flea market in Amphoe Meaung, Amphoe Sri Bun Reung and Amphoe Na Klang, Nong Bua Lum Phu Province," The 1st national conference, July 29, 2016, Ubonratchathani, Thailand. pp. 1621-1628.

[4] L. Gram. "Microbiological spoilage of fish and seafood products," In Compendium of the Microbiological Spoilage of Foods and Beverages". New York: Springer, 2009.

[5] K. Yoshikawa and V. Thonglek, "Research and development of simple detector of nanobubble density through spectroscopic method," The 2nd International Symposium on Application of High-voltage, Plasma & Micro/Nano Bubbles to Agriculture and Aquaculture, July 26th-27th, 2017, Rajamangala University of Technology Lanna, Chiang Mai, Thailand. Available: https://webs.rmutl.ac.th/assets/upload/files/2017/12/20171225115505_23136.pdf

[6] T. Marui, "An Introduction to Micro/Nano-bubbles and their applications," *Systemics, Cybernetics and Informatics*, vol. 11, no. 4, pp. 68-73, 2013.

[7] B. Thongdonphum, W. Pivsa-Art, S. Pivsa-Art, S. Pavasupree, V. Thonglek and K. Yoshikawa, "Effects of Oxygen-free Water on Preservation of Threadfin bream (*Nemipterus hexodon*) & Kuruma prawn (*Penaeus japonicus*)," IJPEST, vol. 12, no. 2, pp. 93-96, 2019.

[8] M. Takahashi, K. Chiba and P. Li, "Free-Radical Generation from Collapsing Microbubbles in the Absence of a Dynamic Stimulus," *J. Phys. Chem. B*, Vol. 111, No. 6, pp. 1343-1347, 2007.

[9] M. Takahashi, K. Chiba and P. Li, "Formation of Hydroxyl Radicals by Collapsing Ozone Microbubbles under Strongly Acidic Conditions," *J. Phys. Chem. B*, No. 39, pp. 11443-11446, 2007.

[10] P. Kwan-on, P. Suwansakornkul, N. Raksakulthai and J. Runglertkreingkrai, "Effect of freshness on physicochemical properties of flesh and protein gel from Spanish mackerel (*Scomberomorus commerson*) during iced storage," Available: http://old.rmutto.ac.th/fileupload/Wannasa%20Balsong6No.5.pdf

[11] A. Imran, J. Chawalit, and K. Somrote, "Characterization of quality degradation during chilled shrimp (*Litopenaeus vannamei*) supply chain," International Food Research Journal, Vol. 20, No. 4, pp. 1833-1842, 2013.

[12] N. Huy Quang, "Guidelines for handling and preservation of fresh fish for further processing in Vietnam," Quality Assurance Department, Seafood Export and Quality Improvement Program, Vietnam, 2005.

[13] FAO, "Improved fresh fish handling methods," Food and Agriculture Organization of the United Nations, Available: http://www.fao.org/docrep/V7180E/V7180e08.htm

[14] T. Tsironi, E. Dermesonlouoglou, M. Giannakourou, P. Taouki, "Shelf life modelling of frozen shrimp at variable temperature conditions," *LWT - Food Science and Technology*, Vol. 42, pp. 664-671, 2009.

[15] N. Khunsoongnern, "Quality change of Tilapia fillet stored under modified atmosphere," Master of Science in Food Technology, Suranaree University of Technology, 2003.

[16] P. Munsch-Alatossava and T. Alatossava, "Nitrogen gas flushing can be bactericidal: the temperature-dependent destiny of *Bacillus weihenstephanensis* KBAB4 under a pure N_2 atmosphere," Frontiers in Microbiology, vol. 5, 1-11, 2014.

[17] A.A. Edris, F.S. Hassanien, F.A.E. Shaltout, A.H. Elbaba and N.M. Adel, "Microbiological evaluation of someheat treated fish products in Egyptian markets," EC Nutrition 12.3, pp. 124-132, 2017.

[18] A. Serizawa, "Fundamentals and Applications of Micro/Nano Bubbles," The 1st International Symposium on Application of High voltage, Plasmas & Micro/Nano Bubbles to Agriculture and Aquaculture (ISHPMNB 2017), January 5-7, 2017, Rajamangala University of Technology Lanna, Chiang Mai, Thailand. Available : http://webs.rmutl.ac.th/assets/upload/files/2017/01/20170106155252_97638.pdf

Improved Particle Swarm Optimization for Optimal Power Flow Problem

Jirawadee Polprasert*
Department of Electrical and Computer Engineering
Faculty of Engineering, Naresuan University
Phitsanulok, Thailand

Abstract: This paper proposes an improved particle swarm optimization (iPSO) for solving optimal power flow (OPF) with non-convex functions. The objective of OPF problem is to minimize generator fuel cost considering voltage stability index subject to power balance constraints and generator operating constraints, transformer tap setting constraints, shunt VAR compensator constraints, load bus voltage and line flow constraints. The proposed iPSO method is an improved PSO by chaotic weight factor and led by pseudo-gradient search for particle's movement in an appropriate direction. Test results on the IEEE 30-bus system indicate that iPSO method is better than other methods in terms of lower generator fuel cost, and lower voltage stability index.

***Keyword*—Pseudo-Gradient Search, Chaotic Weight Factor, Particle Swarm Optimization, Optimal Power Flow, Voltage Stability Index.**

I. INTRODUCTION

Optimal power flow (OPF) is to determine the optimal settings of control variables including real power generation outputs, generator bus voltages, tap setting of transformer and shunt VAR compensators outputs to minimize the generator fuel cost function subject to power balance, and generator operating and network constraints. The objective functions are generation fuel cost with valve-point loading effects and voltage deviation for voltage profile improvement while satisfying the power flow equations, generator bus voltage, real power generation output and reactive power generation output, transformer tap setting, shunt VAR compensators, load bus voltages, and transmission line loadings constraints. OPF has long been developed for on-line operation and control of power system.

So far, various conventional programming techniques such as Newton's method, gradient-based methods, linear programming (LP), nonlinear programming (NLP), quadratic programming (QP), and interior point methods (IPMs) [1-6] have been applied to solve OPF problems. Even though these methods can quickly find a solution, they are highly sensitive to the starting points and may converge prematurely. Moreover, these methods cannot handle non-convex objective function. Therefore, these techniques may not be practical because of nonlinear characteristics of objective function and constraints. To overcome these difficulties, the artificial intelligence and evolutionary based methods including improved genetic algorithm (IGA) [1], improved evolutionary programming (IEP), tabu search (TS) [2], simulated annealing (SA) [3], gravitational search algorithm (GSA) [19], biogeography-based optimization (BBO) [23] were proposed to solve OPF problems. However, the solutions were still far from the optimal solutions.

Recently, PSO has been proposed for solving economic dispatch (ED) [2,5,6-8], reactive power dispatch (RPD) [9-11], optimal power flow (OPF), and optimal location of FACTs devices [12-14]. PSO with time-varying inertia weighting factor (PSO-TVIW), PSO with time-varying acceleration coefficients (PSO-TVAC), self-organizing hierarchical PSO with TVAC (SPSO-TVAC) [16], PG-PSO [17,20], and stochastic weight trade-off PSO (SWT-PSO) [18] have been proposed to obtain better and faster solutions of OPF problem. In addition, the pseudo-gradient based PSO (PG-PSO) method was also applied for solving optimal reactive power dispatch (ORPD) [17] and ED problem [21]. The PG-PSO is based on SPSO-TVAC with guiding position by using pseudo-gradient (PG) for searching the suitable direction towards the optimal solution. The PG-PSO method uses constant weighting factor which may not be effective in solving optimal power flow analysis.

In this paper, an improved particle swarm optimization (iPSO) algorithm is proposed with new linearly chaotic weighting factor and pseudo gradient search algorithm. The proposed iPSO method is tested on the IEEE 30-bus system with objective function including quadratic fuel cost function with voltage stability index. The obtained results is compared with

Manuscript received June 25, 2020; revised June 28, 2020; accepted June 29, 2020. Date of publication June 30, 2020.
*Corresponding author: Asst. Prof. Dr. Jirawadee Polprasert is with Department of Electrical and Computer Engineering Faculty of Engineering, Naresuan University Phitsanulok, Thailand (Email: jirawadeep@nu.ac.th).

PSO-TVIW, and other algorithms.

The organization of this paper is as follows: Section II describes the OPF problem formation. Improved Particle Swarm Optimization is proposed in Section III. The proposed iPSO algorithm is explained in Section IV. Simulation results of OPF problem using the proposed iPSO method on the IEEE 30-bus system is demonstrated in Section V. Finally, Section VI concludes the paper.

II.OPF PROBLEM FORMULATION

Mathematically, the OPF problem can be formulated as follows:

Minimization of Generator fuel cost with voltage stability index

$$F_T = \sum_{i=1}^{NG}\left(a_i + b_i P_{Gi} + c_i P_{Gi}^2\right) + w_f \times L_{\max} \quad (1)$$

$$L_{\max} = \max\left(L_j\right) = \max\left(\left|1 - \sum_{i=1}^{NG} F_{ji}\frac{V_i}{V_j}\right|\right) \quad (2)$$

Subject to

a. Power balance constraints

$$P_i(V,\theta) = P_{Gi} - P_{Di} = \sum_{j=1}^{NB} V_i V_j \left(G_{ij}\cos\theta_{ij} + B_{ij}\sin\theta_{ij}\right) \quad (3)$$

$$Q_i(V,\theta) = Q_{Gi} - Q_{Di} = \sum_{j=1}^{NB} V_i V_j \left(G_{ij}\sin\theta_{ij} + B_{ij}\cos\theta_{ij}\right)$$

$$i = 1,...,NB \quad (4)$$

b. Generator constraints

$$V_{Gi}^{\min} \le V_{Gi} \le V_{Gi}^{\max}, \quad i = 1,....,NG \quad (5)$$

$$P_{Gi}^{\min} \le P_{Gi} \le P_{Gi}^{\max}, \quad i = 1,....,NG \quad (6)$$

$$Q_{Gi}^{\min} \le Q_{Gi} \le Q_{Gi}^{\max}, \quad i = 1,....,NG \quad (7)$$

c. Transformer tap setting constraints

$$t_i^{\min} \le t_i \le t_i^{\max}, \quad i = 1,....,NT \quad (8)$$

d. Shunt VAR compensator constraints

$$Q_{ci}^{\min} \le Q_{ci} \le Q_{ci}^{\max}, \quad i = 1,....,NC \quad (9)$$

e. Voltage limit and line flow constraints

$$V_{Li}^{\min} \le V_{Li} \le V_{Li}^{\max}, \quad i = 1,....,NLB \quad (10)$$

$$S_{li} \le S_{li}^{\max}, \quad i = 1,....,NTL \quad (11)$$

The vectors of dependent/state variables (x) can be represented as:

$$x = \left[P_{G1}, V_{L1}....V_{LNLB}, Q_{G1}....Q_{GNG}, S_{l1}....S_{lNTL}\right] \quad (12)$$

Similarly, the vector of control variables (u) can be expressed as:

$$u = \left[P_{G2}....P_{GNG}, V_{G1}....V_{GNG}, Q_{C1}....Q_{CNC}, t_1...t_{NT}\right] \quad (13)$$

To handle the inequality constraints, the dependent or state variables including power generation output at slack bus (P_{G1}), voltages at load buses (V_{Gi}), reactive power generation output (Q_{Gi}), and transmission line loadings (S_{li}) are incorporated in the objective function as a quadratic penalty function method. Thus, the fitness function ($FitFunc_i$) with the extended objective function can be represented as:

$$\begin{aligned} FitFunc_i = F_i &+ K_S\left(P_{GS} - P_{GS}^{\lim}\right)^2 + K_V\left(V_{Li} - V_{Li}^{\lim}\right)^2 \\ &+ K_Q\left(Q_{Gi} - Q_{Gi}^{\lim}\right)^2 + K_T\left(S_{li} - S_{li}^{\lim}\right)^2 \end{aligned} \quad (14)$$

The limits of dependent or state or control or output variables ($x^{\lim}$) are given as:

$$x^{\lim} = \begin{cases} x^{\max}; & x > x^{\max} \\ x^{\min}; & x < x^{\min} \end{cases} \quad (15)$$

III. iPSO ALGORITHM

In the conventional PSO method, a population of particles moves in the search space. During the process, each particle is randomly adjusted according to its own experiences and neighbor's experience of particles. The velocity of particles is changed over time and their positions will be updated accordingly. Mathematically, in d-dimension optimization problem, the velocity and position of each particle can be updated as follows:

$$\begin{aligned} v_{id}^{k+1} = \omega^k v_{id}^k &+ c_1 \times rand_1 \times \left(pbest_{id}^k - x_{id}^k\right) \\ &+ c_2 \times rand_2 \times \left(gbest_d^k - x_{id}^k\right) \end{aligned} \quad (16)$$

$$x_{id}^{k+1} = x_{id}^k + v_{id}^{k+1} \quad (17)$$

$$i = 1,....,np; \quad d = 1,....,nd$$

$$\omega^k = \omega_{\max} - \left(\omega_{\max} - \omega_{\min}\right) \times \frac{k}{k_{\max}} \quad (18)$$

The main objective of the proposed iPSO method is to employ chaotic weighting factor to find the proper velocity updating for accelerating the search for global optimal solution. Here, the combined pseudo-gradient and PSO with chaotic weight factor is proposed. The updating position of particles between two points, x_a and x_b corresponding to x_k and x_{k+1}, respectively can be rewritten as follows:

$$x_{id}^{k+1} = \begin{cases} x_{id}^{k} + \alpha \times \phi\left(x_{id}^{k+1}\right) \times \left|v_{id}^{k+1}\right| & if \quad p_g\left(x_{id}^{k+1}\right) \neq 0 \\ x_{id}^{k} + v_{id}^{k+1} & otherwise \end{cases} \quad (19)$$

From (19), if the pseudo-gradient is non-zero, the involved particle's position is speeded up to the global optimal solution by its enhanced velocity; otherwise, the position is generally updated by (17). The value of can be adjusted so that a particle can move faster or slower depending on the characteristic of individual problem. In fact, if the value of is too large, it may not to lead to optimal solution because particles are stuck at their limit positions. On the other hand, too small value of may lead particles being trapped in local minima in the search space. In this paper, the proper value of should be tuned in the range [1,10].

Chaotic Weighting Factor

For determining the inertia weight factor, the inertia weight is modified by using *logistic map* equation as following [22]:

$$\eta^{k} = 4 \times \eta^{k-1} \times \left(1 - \eta^{k-1}\right) \quad (20)$$

To improve capability of global searching solution and escape the local minimum, the new weighting factor is applied to chaotic sequence which can be modified as follows:

$$c\omega^{k} = \omega^{k} \times \eta^{k} \quad (21)$$

In Eq. (23), the initial η^{0} should be in range [0,1] and $\eta^{0} \notin \{0, 0.25, 0.5, 0.75, 1.0\}$.

Pseudo-gradient search

Suppose that the movement of particle in each *d*-dimension, $x_a = [x_{a1}, x_{a2}, \ldots, x_{and}]$ is a point in the search space and moves to another point x_b.

Case 1: If $f(x_b) < f(x_a)$, the direction from x_a to x_b is positive direction. The pseudo-gradient at point x_b can be determined by:

$$p_g\left(x_b\right) = \left[\phi\left(x_{b1}\right), \phi\left(x_b\right), \ldots, \phi\left(x_{bnd}\right)\right]^{T} \quad (22)$$

$$\phi\left(x_{bd}\right) = \begin{cases} 1 & if \quad x_{bd} > x_{ad} \\ 0 & if \quad x_{bd} = x_{ad} \\ -1 & if \quad x_{bd} < x_{ad} \end{cases} \quad (23)$$

Case 2: If $f(x_a) \geq f(x_b)$, the direction from x_a to x_b is negative direction. The pseudo-gradient at point x_b can be determined by:

$$p_g\left(x_b\right) = 0 \quad (24)$$

If the pseudo gradient at point *b*, $p_g(x_b)$ is not equal to zero, it implies that the pseudo gradient could find a better solution in the next step which is based on direction indicator. Otherwise, the search direction at that point should not be changed.

IV. Procedure of Proposed iPSO Method

The proposed IPG-PSO procedure can be described as follows:

Step 1: Initialization of swarm
Step 2: Run power flow and evaluate fitness function
Step 3: Determining *pbest* and *gbest*
Step 4: Updating velocity
Step 5: Update position
Step 6: Update pbest and gbest
Step 7: Stopping criteria

The flowchart of the proposed IPG-PSO method is shown in Fig. 1

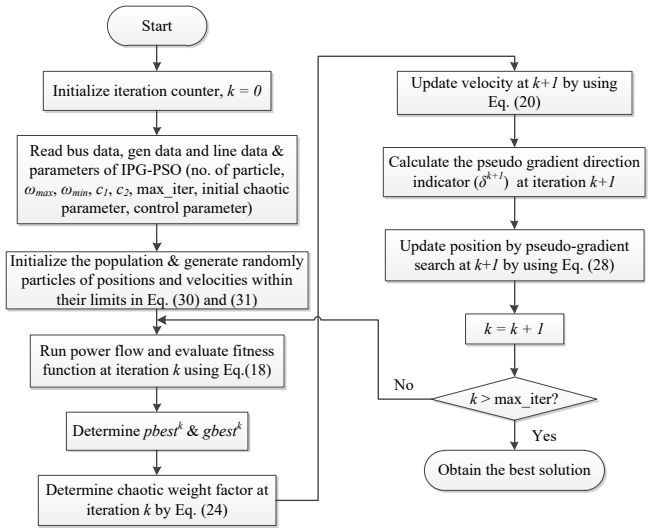

Fig. 1 Flow Chart of Proposed iPSO Algorithm

V. Simulation Result

The proposed iPSO method has been tested on the IEEE 30-bus system for solving OPF problem considering quadratic generator fuel cost function with voltage stability index. The proposed method is run 50 independent trials and the obtained results are compared to those from different PSO and other methods. The coding has been written and implemented in MATLAB computing environment. The data for IEEE 30-bus system can be found [24].

The characteristics and data for the base case of the test system are given in Table 1. The load bus voltages are limits in the range [0.95-1.10] p.u.

Table 1. Characteristics of IEEE 30-bus system

No. of generators	No. of transformers	No. of branches	No. of capacitor banks	No. of control variables	IEEE 30-bus system
6	4	41	9	19	
$\sum P_{Di}$ (MW)	$\sum Q_{Di}$ (MVar)	$\sum P_{Gi}$ (MW)	$\sum Q_{Gi}$ (MVar)	P_{Gmax} (MW)	Q_{Gmax} (MVar)
283.4	126.2	287.93	66.32	4.533	23

In this paper, the power flow solutions are obtained from MATPOWER toolbox (MATPOWER). For comparison, PSO-TVIW method is applied to solve OPF problem.

In this case, the objective function is to minimize the total fuel cost with the voltage stability index for enhancing voltage stability.

Table 2. Result comparison with other PSO method on the IEEE 30-bus system

Control Variable	PSO-TVIW	iPSO
Min. *Cost*+L_{max} ($/h)	809.7497	798.5600
Avg. *Cost*+L_{max} ($/h)	809.8829	799.6737
Max. *Cost*+L_{max} ($/h)	810.0436	801.7935
SD	0.0056	0.0034
Min L_{max}	0.1222	0.1083
P_{loss} (MW)	16.1567	16.0349
CPU Time(s)	10.53	10.06

Table 3. Result comparison with other methods on the IEEE 30-bus System

Methods	Total cost ($/hr)	L_{max} (p.u.)	CPU time (sec)
PSO [15]	801.16	0.1246	-
TLBO [31]	799.978	0.1131	-
BBO [23]	-	0.1104	16.29
DE [20]	-	0.1219	-
iPSO	798.56	0.1083	10.06

In Table 2 and Table 3, it is observed that the proposed iPSO method yields lower minimum and average L-index than PSO [2], BBO [15], TLBO [19], and other PSO methods in a slightly faster computing time.

VI. Conclusion

In this paper, an improved particle swarm optimization (iPSO) method has been efficiently solving OPF problems considering objective function including generator fuel cost function with voltage stability index. The features of iPSO include linearly chaotic weighting factor to avoid trapping in the local minimum and pseudo-gradient to better guide particles in the search space. Test results on the IEEE 30-bus system indicates that the proposed iPSO method can obtain a higher solution quality than other methods, leading to generator fuel cost savings with voltage stability enhancements.

References

[1] L.L. Lai and J.T. Ma, "Improved genetic algorithms for optimal power flow under both normal and contingent operation states," *Int. J. Elect. Power Energy Syst.*, vol. 19, no. 5, pp. 287-292, 1997.

[2] M.A. Abido, "Optimal power flow using tabu search algorithm," *Electric Power Components and Systems*, vol. 30, no. 5, pp. 469-483, 2002.

[3] C.A. Roa-Sepulveda and B.J. Pavez-Lazo, "A solution to the optimal power flow using simulated annealing," *Int. J. Electrical Power and Energy Systems*, vol. 25, no.1, pp. 47-57, 2003.

[4] J. Kennedy and R.C. Eberhart, "Particle swarm optimization," *In Proceedings of IEEE International Conference on Neural Networks*, Perth, Australia, 1995, vol.4, pp.1942-1948.

[5] A.A. Abou El Elaa and M.A. Abido, "Optimal Operation Strategy for Reactive Power Control Modeling," *Simul. Control, Part A*, vol. 41, no.3 pp. 19-40, 1992.

[6] K. Thanushkodi and et.al., "An efficient particle swarm optimization for economic dispatch problems with non-smooth cost functions," *WSEAS Trans. Power Systems*, vol .4, no. 3, pp. 257-266, 2008.

[7] J.B. Park and et.al., "An improved particle swarm optimization for economic dispatch problems with non-smooth cost functions," *IEEE Power Engineering Society General Meeting*, 2006.

[8] C.H. Chen and S.N. Yeh, "Particle swarm optimization for economic power dispatch with valve-point effects," *In Proceedings of IEEE PES Transmission and Distribution Conference and Exposition Latin America*, Venezuela, 2006.

[9] K.T. Chaturvedi, M. Pandit, and L. Srivastava, "Self-organizing hierarchical particle swarm optimization for nonconvex economic dispatch," *IEEE Trans. Power Systems*, vol. 23, no. 3, pp. 1079-1087, 2008.

[10] H. Yoshida and et.al., "A particle swarm optimization for reactive power and voltage control considering voltage security assessment," *IEEE Trans. on Power Systems*, vol .15, no. 4, pp. 1232-1239, 2001.

[11] G. Krost, G.K. Venayagamoorthy, and L. Grant, "Swarm intelligence and evolutionary approaches for reactive power and voltage control," *IEEE Swarm Intelligence Symposium*, September 21-23, 2008.

[12] K.S. Swarup, "Swarm intelligence approach to the solution of optimal power flow," *Indian Institute of Science*, pp. 439–455, 2006.

[13] A.A.A. El-Ela and R.A-A. El-Sehiemy, "Optimized generation costs using modified particle swarm optimization version," *Wseas Trans. Power Systems*, pp. 225-232, 2007.

[14] S. Sutha and N. Kamaraj, "Optimal location of multi type FACTS devices for multiple contingencies using particle swarm optimization," *International Journal of Electrical Systems Science and Engineering*, vol. 1, no. 1, pp. 16-22, 2008.

[15] A. Bhattacharya and P.K. Chattopadhyay "Application of biogeography-based optimization to solve different optimal power flows," *IET Gener. Transm. Distrib.*, vol. 5, no. 1, pp. 70-80, 2011.

[16] A. Ratnaweera and S.K. Halgamuge, "Self-Organizing Hierarchical Particle Swarm Optimizer with Time-Varying Acceleration Coefficients," *IEEE Trans. on Evolutionary Computation,* vol. 8, no. 3, pp. 240-255, 2004.

[17] D.A. Le and V.N. Dieu, "Optimal Reactive Power Dispatch by Pseudo-Gradient Guided Particle Swarm Optimization," *In proceedings of IPEC, 2012 Conference on Power & Energy*, pp. 7-12, 2012.

[18} S. Chalermchaiarbha and W. Ongsakul, "Stochastic Weight Trade-Off Particle Swarm Optimization for Nonconvex Economic Dispatch," *Energy Conversion and Management,* 70, 66-75, 2013.

[19] H.R.E.H. Bouchekara, M.A. Abido, and M. Bouchekara, "Optimal Power Flow using Teaching-Learning-Based Optimization Technique," *Electric Power Systems Research,* vol. 114, pp. 49-59, 2014.

[20] V.N. Dieu and P. Schegner, "An Improved particle swarm optimization for optimal power flow,". In P. Vasant (Ed.), *Meta-Heuristics Optimization Algorithms in Engineering, Business, Economics and Finance,* Hershey, PA: IGI Global, pp. 1-40, 2012.

[21] L.L. Dinh, V.N. Dieu, and P. Vasant, "Artificial Bee Colony Algorithm for Solving Optimal Power Flow Problem," *Research Article: The Scientific World Journal*, pp. 1-9, 2013.
[22] R. Caponetto, L. Fortuna, S. Fazzino, and M.G. Xibilia, "Chaotic sequences to improve the performance of evolutionary algorithms," *IEEE Trans. Evol. Computat.,* vol. 7, no. 3, pp. 289-304, 2013.

Risk Assessment of HV Transmission Lines Using Failure Mode, Effect, and Criticality Analysis

Cattareeya Suwanasri*[1], Surapol Saribut[1], Waraporn Luejai[2] and Thanapong Suwanasri[2]
[1]Faculty of Engineering, [2]The Sirindhorn International Thai-German Graduate School of Engineering
King Mongkut's University of Technology North Bangkok
1518 Pracharat Sai 1, Wongsawang, Bangsue
Bangkok, Thailand

Abstract: The effective transmission management is of prime importance to gain a better quality of electricity under lower cost and capital investment. So, an asset management focuses on cost reduction, condition-based maintenance requires a modern database to support usage and including a need for appropriate risk management in order to receive the highest return and the most worthwhile in HV transmission line usage. Presently, large number of transmission lines is aged and gradually degraded. Those transmission lines need some reparation, replacement or renovation with new components to prevent a risk to failure that may occur and effect to system reliability, safety, environment, and efficiency of use. This paper introduced the Failure Mode, Effect, Criticality Analysis (FMECA) method to assess the transmission system. The major components include conductor, conductor accessories, insulator, tower, tower accessories, foundation, and lightning protection. The FMECA procedure includes five importance steps as (1) objective setting, (2) failure event identification, (3) risk assessment (4) result evaluation, and (5) risk management. An aged 115 kV transmission lines is assessed as example. The final evaluated result is presented in 4 different color bands as red, orange, yellow, and green, which represent very high risk, high risk level, moderate risk, and low risk level, respectively to effective planning and maintenance.

***Keyword*— Risk assessment, risk matrix, renovation index, FMECA, transmission line.**

I. INTRODUCTION

Nowadays, electricity demand keeps increasing while electrical power system has been developed continuously. Modern electrical power transmission focuses on effective operation with cost reduction. Therefore, a condition-based maintenance and risk management are major concerns affecting to power transmission efficiency [1-4]. HV transmission lines in Thailand consists of three different levels such as 115, 230, and 500 kV. Normally, they have a long-distance for transmitting electricity to each region in Thailand. There were blackouts caused by topology, pollution, disasters, overload condition, and equipment deterioration. The natural failure causes are mostly uncontrollable. However, a deterioration of transmission system can be controlled leading to lower failure event.

The condition-based maintenance and risk assessment are introduced for Failure Mode, Effect, and Criticality Analysis (FMECA) [5]. It is a famous method to analyse the risk by considering the failure of equipment in the system. The FMECA involves various effects such as finance, safety, environment, and efficiency and bring them to analyze a critical level of system. The FMECA process examines effects in order to lower failure level as well as recommend actions or compensating provision to reduce number of failures. So, the maintenance and the risk in the use of each equipment can be managed effectively.

Therefore, this paper proposes the FMECA for HV transmission lines, risk assessment, and appropriate maintenance planning. The research aims to apply FMECA with all technical information, finance, environment, social effect, and etc. of transmission lines, to understand method of assessment condition and risk of usage, to be able to analyse and manage the risk as well as appropriate maintenance planning of transmission lines.

The analysing procedure includes five steps as (1) objective setting, (2) failure event identification, (3) risk assessment (4) result evaluation, and (5) risk management.

Manuscript received June 10, 2020; revised June 23, 2020; accepted June 27, 2020. Date of publication June 30, 2020.

*Corresponding author: Cattareeya Suwanasri, Faculty of Engineering, King Mongkut's University of Technology North Bangkok, Bangkok, Thailand (Email: cattareeya.s@eng.kmutnb.ac.th)

II. Failure Mode, Effect, and Criticality Analysis (FMECA) for Transmission Lines

In Fig. 1, HV overhead transmission line is classified into eight components consisting of conductor, conductor accessories, insulator, steel structure, foundation, lighting protection system, tower accessories, and right of way as given in Table 1 [6]. The sub-components of each component are also presented. However, right of way is ignored in the risk assessment in this paper. An aged 115 kV transmission lines is analyzed by using FMECA via Microsoft Excel program.

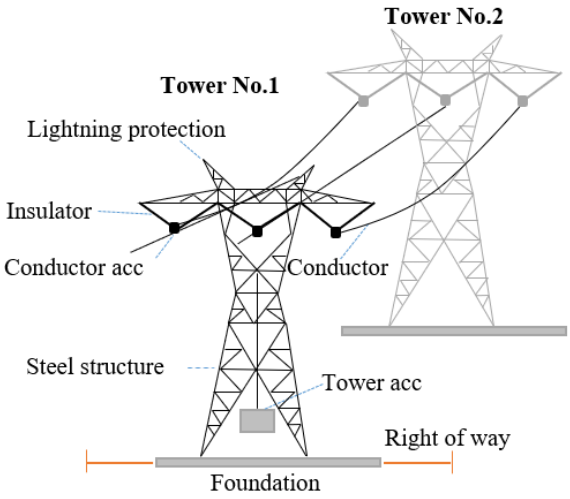

Fig.1. Components of the transmission line.

TABLE I
Components of OHL Evaluation.

Components	Sub-components
Conductor (C)	Conductor
Cond. accessories (CA)	Spacer, Damper, Joint, Dead End, PG Clamp
Insulator (IN)	Insulator, Fittings, Arrester
Tower (T)	Structure, Anchor and Guy
Foundation (D)	Concrete Foundation, Grillage Foundation, Stub
Lightning protection (LP)	OHGW/OPGW, OHGW Fitting, Marker, Grounding
Tower accessories (TA)	Danger Sign, Tower Number Sign, Phase Plate
Right of way (RoW)	Right of way

After the analysis, the result of FMECA is presented in a criticality matrix as shown in Fig. 2. The evaluated results are presented in a criticality matrix as shown in Fig. 1. It is differentiated into four color bands as red, orange, yellow, and green, which represent very high risk, high risk level, moderate risk, and low risk level, respectively. The numbers 1 to 25 represent the severity from low to high. The black dots show the risk of transmission components that may fall in different colors depending to their conditions and risks.

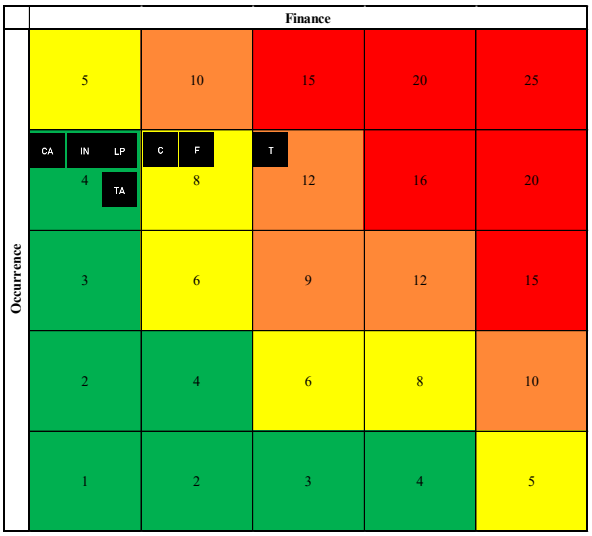

Fig. 2. Criticality matrix.

The FMECA considers the risk of all sub-components of HV transmission line. The risk based on severity in four criteria as efficiency, safety, environment, and finance. Then all criteria are analyzed. The critical value of the HV transmission line system as follows.

III. Severity on Efficiency

Efficiency is considered from condition of transmission equipment. The inspection and special tests for assessing the conditions of HV transmission sub-components of each group is needed to evaluate. The weighting and scoring method (WSM) is applied for evaluation while Analytical Hierarchy Process (AHP) method [7-8] is used to determine the weight of each criterion [7-8]. Example of certain types of tests as in Table III to IX [10-14]. The score used to classify sub-components' condition is divided into 5 levels as 0 (very good condition), 1 (good), 2 (moderate), 3 (bad) and 4 (very bad).

TABLE II
Evaluation Criteria for Torsional Ductility

Score	Torsional Ductility
0	Remaining Torsional Ductility > 15
1	12 < Remaining Torsional Ductility < 15
2	8 < Remaining Torsional Ductility < 12
3	5 < Remaining Torsional Ductility < 8
4	Remaining Torsional Ductility < 5

TABLE III
Evaluation Criteria for Resistance Measurement of Joint

Score	Resistance Measurement
0	Resistance not more than 30% from new condition.
2	Resistance not more than 50% from new condition.
4	The resistance of joint is equal to or greater than resistance of conductor of the same length.

2nd Revision, June 23, 2020
*corresponding authors: Cattareeya Suwanasri, Faculty of Engineering, King Monkut's University of Technology North Bangkok, Bangkok, Thailand. Email: cattareeya.s@eng.kmutnb.ac.th.

TABLE IV
EVALUATION CRITERIA FOR VISUAL INSPECTION OF COMPOSITE INSULATOR

Score	Visual Inspection of Composite Insulator
0	New condition, surface of hydrophobicity is in HC1.
1	Surface of hydrophobicity is in HC2.
2	Insulator has small rust. Hydrophobicity is in HC3.
3	Fitting has small rust. Hydrophobicity is in HC4.
4	Ball and pin loss of metal. Cross-sectional area decrease more than 16%.
5	Flashover occurs severe. Don't pass electrical test.

TABLE V
EVALUATION CRITERIA FOR VISUAL INSPECTION OF STEEL POLE

Score	Visual Inspection of Steel Pole
0	New condition, surface is smooth and doesn't damage.
2	Surface of zinc has small rust.
3	Connector of cross arm has medium rust.
5	Connector of cross arm occur severe rust.

TABLE VI
EVALUATION CRITERIA FOR VISUAL INSPECTION OF STEEL STUB

Score	Visual Inspection of Steel Stubs
0	New condition.
1	Galvanize of stub has gray color.
2	Connector of stub has rust.
3	Stub and concrete occur pitting rust
5	Concrete fall out of steel stub.

TABLE VII
EVALUATION CRITERIA FOR LOSS OF TENSILE STRENGTH OF OHGW

Score	Loss of Tensile Strength of OHGW
0	Remaining Tensile Strength > 100% RTS
2	95% RTS < Remaining Tensile Strength < 100% RTS
3	90% RTS < Remaining Tensile Strength < 95% RTS
4	85% RTS < Remaining Tensile Strength < 90% RTS
5	Remaining Tensile Strength < 85% RTS

TABLE VIII
EVALUATION CRITERIA FOR VISUAL INSPECTION OF PHASE IDENTIFICATION

Score	Visual Inspection of Phase Identification
0	Good condition.
3	Color of label is noticeably blurred.
5	Color of label is very fuzzy, cracked, loose fitting.

The equation used to calculate the percentage of condition %CI of the component are given in Eq. (1) [4].

$$\%CI_{component} = \frac{\sum_{i=1}^{M}(S_i x W_{sub-component,i})}{\sum_{i=1}^{M}(S_{max} x W_{sub-component,i})} x\,100 \quad (1)$$

where S_i is the score, S_{max} is the maximum score of each sub-component, $\%W_{sub-component,i}$ is the important weight of sub-component i^{th} while M is the number of sub-components of each component.

The $\%CI_{component,j}$ includes conductor ($\%CI_C$), conductor accessories ($\%CI_{CA}$), insulator ($\%CI_I$), steel structure ($\%CI_{SS}$), foundation ($\%CI_F$), lighting protection ($\%CI_{LP}$), tower accessories ($\%CI_{TA}$), and right- of-way ($\%CI_{RW}$).

From Eq. (1), $\%CI_{component,j}$ of each component is further used to calculate the %TRI of tower as shown in Eq. (2) [4].

$$\%TRI = \frac{\sum_{j=1}^{N}(\%CI_{component,j} x W_j)}{\sum_{j=1}^{N}(\%CI_{component,j,max} x W_j)} x\,100 \quad (2)$$

where $\%CI_{component,j,max}$ is the maximum of each $\%CI_{component,j}$, the $\%W_j$ is the important weight of component j^{th} and N is a total number of component.

The overall procedure to calculate the component health index is shown in Fig. 3.

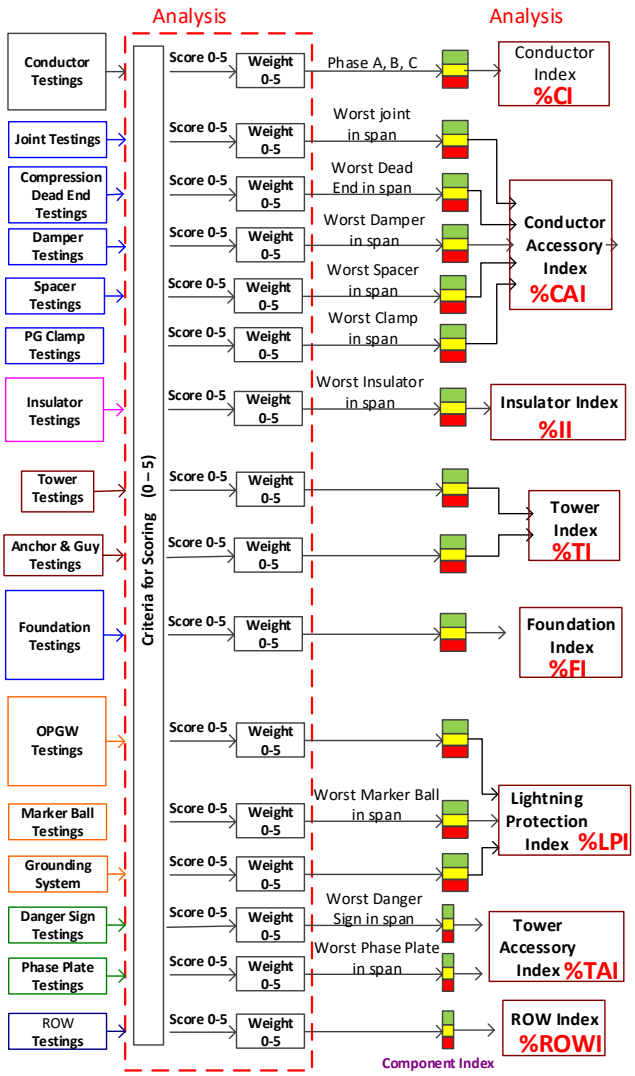

Fig. 3. Condition assessment of transmission line in transmission system.

The scores interpreted to %HI, its condition and maintenance strategy are explained in Table IX. [15-16]

TABLE IX
MAINTENANCE STRATEGY VS CONDITIONS

Score	Description	Maintenance Strategy
1	very good	Normal condition, normal preventive maintenance
2	good	Normal condition, normal preventive maintenance
3	moderate	Increasing scheduled maintenance, medium term plan to renovate/replace
4	degradation	Needs replacement of defective equipment, short term replacement planning by new OHL
5	end of life	Urgent need to replacement of defective equipment

TABLE X
SUB-CRITERIA FOR ENVIRONMENT

Criteria	Score				
	Very Low (1)	Low (2)	Moderate (3)	High (4)	Very High (5)
Age of transmission lines (%)	0-10	11-20	21-25	26-30	>30
Impact on electricity users	general provinces				industrial estates, large province/ tourist attractions/ important business districts
Pollution and location		agri-cultural	plant firing area	animal area	coast area /industrial area
Impact on communities and public image		normal			compact line

TABLE XI
SUB-CRITERIA FOR SAFETY/RELIABILITY

Criteria	Score				
	Very Low (1)	Low (2)	Moderate (3)	High (4)	Very High (5)
Load percentage (%)	0-20	21-30	31-40	41-50	>50
System usage		no tie line		radial line	tie line /rapid load shedding /generator connected
Voltage levels (kV)		≤ 115		230	500/300 kVDC
Contingency analysis	normal		N-2		N-1

IV. SEVERITY ON ENVIRONMENT [16-18]

Severity on environment involves 4 sub-criteria as age, impact on electricity users, pollution and use of areas near the line of wiring, and impact on communities and organization image described as follows.

A. Age of HV Power Transmission Line

It reflects the invisible deterioration and the likelihood of power outages of HV transmission lines that have a long service life or designed specifications that are lower than the present conditions of use, such as thin, easily damaged metal frame, withstand wind tolerance.

B. Impact on Electricity Users

Impact on electricity users involves the importance of the load or the area where the HV power line is being supplied. It is an assessment that if there are problems with the HV transmission line, leading to how much it will affect the electricity users. By considering the importance level according to the type of electricity users, the impact is divided into 3 groups; industrial estates, large provinces/tourist attractions/important business districts, and general provinces.

C. Pollution

It is a matter of pollution level at the location where the HV transmission line is installed, i.e. dusty/sea vapour area, chemical industry causing flashover problems on the insulator surface, corrosive corrosion on the iron core, etc. Therefore, the level of pollution at the installation location are important.

D. Impact on Communities and Organization Image

It is an assessment that if HV transmission lines affect communities near the power line. This affects the public image of utility. Then a considering on some limitation of design and installation distance of the power line is a prime concern.

The scores relevant to the conditions of four sub-criteria for environmental severity are details in Table XI.

V. SEVERITY ON SAFETY/RELIABILITY [19-20]

Similarly, safety/reliability criterion involves four sub-criteria as load percentage, system usage, voltage levels, and contingency analysis (N-1 criteria) described as follows.

A. Load Percentage

Calculated from the highest load of the HV transmission line in the month of the highest electricity demand in each year compared to the Rated Power (MVA) of the HV transmission line, because in the case of HV transmission lines, there is a problem of not being able to supply power HV transmission lines with a higher percentage of a load will have a wider impact than HV transmission lines with a lower load percentage.

B. System Usage

It is a consideration of the importance of using HV transmission lines in power systems by considering whether the transmission lines that are used to connect the power plant to the power system are using a tie line or with a rapid load shading setting.

C. Voltage Level

Voltage levels can be referred power transmitted through HV transmission line in order to compare the impact on the electrical system HV transmission lines that operate at HV levels have a large amount of power.

D. Contingency Analysis (N-1 Criteria)

It is considered that if the HV power lines installed in

use in various circuits there is a problem with the electrical system, which will affect the ability to send electric power. HV transmission lines with N-1 circuits will cause the system to be more affected than HV power lines with N-2. The scores relevant to the conditions of four sub-criteria for safety/reliability severity are details in Table XII.

Finally, the scores from sub-criteria in environment as well as in safety/reliability must be combined into a single score for the environment as well as for the safety/reliability to calculate the possibility of failure concurrence. To determine the score for the environment as well as for the safety/reliability, 4 conditions to combine into single score as shown in the Table XII. For more understanding, example to combine and obtain the single score is expressed in Table XIII.

TABLE XII
COMBINING TO A SINGLE SCORE FOR ENVIRONMENT AS WELL AS SAFETY/RELIABILITY

Single Score	Description
1	All of scores are 1
2	Two of score 2 and two of score 1
	One of score 2 and three of score 1
3	Two of score 3 and two of score 2,1
	One of score 3 and three of score 2,1
	Three of score 2 and one of score 2,1
4	Two of score 4 and two of score 3,2,1
	One of score 3 and three of score 3,2,1
	Three of score 2 and one of score 3,2,1
5	At least one of score 5
	Three of score 4 and one of score 4,3,2,1

TABLE XIII
SINGLE SCORE FOR ENVIRONMENT CRITERION

Scores of Criteria 1-4				Single Score	Description
1	1	1	1	1	All of scores are 1
1	1	1	2	2	Two of score 2 and two of score 1
1	1	2	2		One of score 2 and three of score 1
1,2	2	2	2	3	Two of score 3 and two of score 2,1
1,2	1,2	1,2	3		One of score 3 and three of score 2,1
1,2	1,2	3	3		Three of score 2 and one of score 2,1
1,2,3	3	3	3	4	Two of score 4 and two of score 3,2,1
1,2,3	1,2,3	1,2,3	4		One of score 3 and three of score 3,2,1
1,2,3	1,2,3	4	4		Three of score 2 and one of score 3,2,1
1,2,3,4	4	4	4	5	At least one of score 5
1,2,3,4	1,2,3,4	1,2,3,4	5		Three of score 4 and one of score 4,3,2,1

VI. SEVERITY ON FINANCE [21-22]

The cost of sub-components must be identified and assessed to determine the finance score for each sub-component as given in Table XIV. For example, the cost is lower than 10% of the total price, the score is "1". Moreover, the exact cost of sub-components must also be involved as presented in Table XV. The percentage (%) of total cost also calculated that can be compared with Table VIII to obtain the score for finance severity analysis.

TABLE XIV
SCORE FOR FINANCE CRITERION

Score	Description
1	Less than 10% of the total price
2	10-29% of the total price
3	30-49% of the total price
4	50-69% of the total price
5	70-100% of the total price

TABLE XV
FINANCE TEST RESULT OF 115 KV

Component	Replacement (Baht/km.)	Percentage (%)
Conductor	900,000	24.035
Conductor accessories	67,500	1.803
Insulator	72,000	1.923
Steel structure	1,800,000	48.071
Foundation	750,000	20.029
Lightning protection	150,000	4.006
Tower accessories	5,000	0.134
Total	3,744,500	100.000

VII. CRITICALITY CALCULATION AND ANALYSIS

In criticality analysis, a probability of failure occurrence needs to be determined. The failure occurrence score for each sub-component can be differentiated in Table XVI. Thereafter, severities based on the efficiency, environment, safety/reliability, and finance are determined. Then, the criticalities of all of them can be calculated by using Eq. (3).

$$\text{Criticality} = \text{Severity} \times \text{Occurrence} \quad (3)$$

TABLE XVI
CRITERIA FOR OCCURRENCE

Score	Description
1	0 failure per year
2	-
3	1-5 failures per year
4	6-10 failures per year
5	>10 failures per year

VIII. RESULT AND DISCUSSION

Calculation steps for criticality of a 115 kV transmission is given as example. After establishing the database from test results, severities in efficiency, environment, safety and finance is evaluated as given in Table XVII.

TABLE XVII
CRITICALITY SCORE OF 115 KV TRANSMISSION LINE

Component of Transmission line	Severity				Occurrence	Criticality			
	Efficiency	Environment	Safety/ Reliability	Finance		Efficiency	Environment	Safety/ Reliability	Finance
Conductor	4	4	4	2	4	16	16	16	8
Conductor Accessories	4	4	4	1	4	16	16	16	4
Insulator	4	4	4	1	4	16	16	16	4
Tower	4	4	4	3	4	16	16	16	12
Foundation	4	4	4	2	4	16	16	16	8
Lightning Protection	4	4	4	1	4	16	16	16	4
Tower Accessory	4	4	4	1	4	16	16	16	4

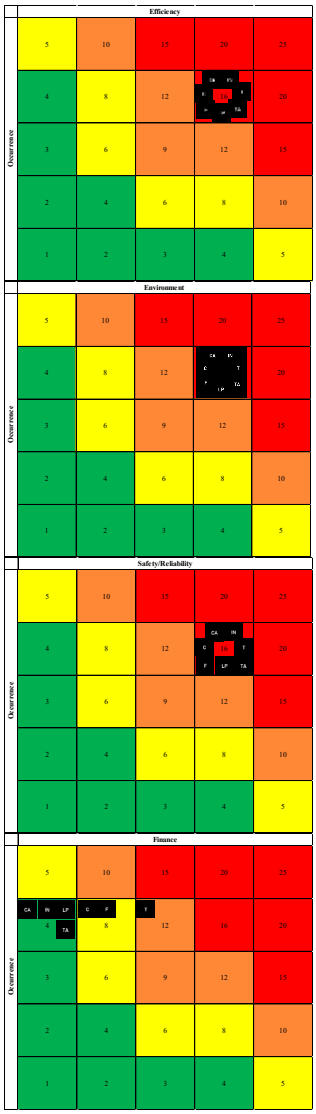

Fig. 4. Criticality matrix of 115 kV transmission line.

The criticality scores of all sub-components and plotted in four criticality matrices of efficiency, environment, safety/reliability and finance as shown in Fig. 4. The criticality is a combination of the severity of each criterion and the frequency of its occurrence. The failure measurement and the need for maintenance and mitigation are as addressed in Table XVIII.

TABLE XVIII
CRITICALITY ANALYSIS

Score	Risk level	Color	Meaning
22-25	Highest	Red	Unacceptable levels need to be expedited to manage the risk to Acceptable level immediately
16-21	High	Orange	Unacceptable level Which must manage the risk in order to be in the next acceptable level
5-15	Medium	Yellow	Acceptable level but there must be control to prevent Risk moving to an unacceptable level
1-4	Low	Green	Acceptable level Without risk control, no additional management

From the results in Table XVIII and Fig. 4, the criticality results in efficiency, environment, and safety/reliability are 16 and all plotted in the red zone. These can be interpreted according to Table XVIII that the line is unacceptable level and needs to be expedited to manage the risk to acceptable level immediately because the transmission line is aged and in bad condition, as well as it is located the important area. However, in finance critically matrix some sub-components are located in a green, yellow and orange because the costs of those sub-components are relatively small percentage out of the cost of overall transmission line.

IX. CONCLUSION

HV transmission lines are aged and has deteriorated according to their usage. These transmission lines need effective improvement. The condition of all components need to be evaluated by using different methods for an effective management. In condition assessment, four severity criteria are considered including efficiency, environment, safety/reliability, and finance. Microsoft excel is used as a simple tool and displays the criticality. An aged 115 kV transmission lines in Thailand was evaluated using FMECA method. The results show that it encounter highest risk in operation because the criticality in efficiency, environment, safety/reliability are in the red zone for all sub-components because the transmission line is aged and in bad condition, as well as it is located the important area. The criticality in finance is in the green, yellow and orange zones because of the costs of are affordable to reparation. FMECA method can be used as an effect tool to assess transmission line in different points of criticality, and finally help the utility to effectively manage with an easy tool, as well as increase work efficiency in maintenance and strengthening of electrical systems to be more reliable and stable with optimal budget.

ACKNOWLEDGMENT

Authors would like to acknowledge the Department of Transmission System Maintenance, Department of Research and Development, the Electricity Generating Authority of Thailand (EGAT) for data analysis and support.

REFERENCES

[1] Cigre SC 22 WG13, "*Working Group Preliminary Report: Management of Existing Overhead OHLs*." Cigre Session 22-107, 2000.

[2] Cigre, "*Ageing of the System Impact on Planning*." Cigre Brochure 176, WG 37.27, 2000.

[3] Cigre, "*Overview of Cigre Publications on Asset Management Topics*. Cigre Technical Report, Electra no. 262, June 2012.

[4] A. Ibrahim and A. Pharmatrisanti, "Transmission line assessment." *In 2012 IEEE International Conference on Condition Monitoring and Diagnosis*. 23-27 September 2012, Bali, Indonesia, 2012.

[5] R. Y. Trianto, M. R. Pahlevi, B. Z. Bardani, "FMECA development in PLN TRANS-JBTB." *2017 International Conference on High Voltage Engineering and Power Systems (ICHVEPS)*, Sanur, Indonesia.

[6] Ittiphong Yongyee, Cattareeya Suwanasri, Thanapong Suwanasri, Waraporn Luejai, "Condition assessment in transmission line asset for maintenance management", *2018 International Electrical Engineering Congress (iEECON)*, 2018, Krabi, Thailand.

[7] T.L. Saaty, "*Relative Measurement and its Generalization in Decision Making: Why Pairwise Comparisons are Central in Mathematics for the Measurement of Intangible Factors-The Analytic Hierarchy/Network Process*." In Review of the Royal Spanish Academy of Sciences, vol. 102, pp. 251-318, 2008.

[8] Tanaka, H., Tsukao, S., Yamashita D., "Multiple criteria assessment of substation conditions by pair-wise comparison of Analytic Hierarchy Process." *IEEE Transactions on Power Delivery*, vol. 25, no.4, pp. 3017-3023, 2010.

[9] Waraporn Luejai, Thanapong Suwanasri, Cattareeya Suwanasri, "Condition evaluation of high voltage transmission line in Thailand." *In the Proceedings of the 21st International Symposium on High Voltage Engineering (ISH 2019)*, pp 171-183, 2019, Budapest, Hungary.

[10] A. Van Der Wal, A.A.H.J. Ross, KEMA TDC, *Condition Assessment of Overhead lines*." Cigre Session B2-204, 2004.

[11] Carlos J. Garcia-Alamo, Jaymi Palacios, *Structural Analysis for Transmission Lattice Steel Tower in the 400 kV transmission lines EL Tablazo – Cuatricenteneario No.1 and 2*." Cigre Session B2-302, 2010.

[12] Cigre WG B2.03, *Guide for the Assessment of Old Cap and Pin and Long-rod transmission line Insulators Made of Porcelain or Glass: What to Check and When to Replace?*." Cigre Technical Report, Electra no. 228, October 2006.

[13] F. Chone, M. Gaudry, J. Parrotta, L. Gourit, B. Larripa, "*Assessment of Existing Overhead transmission lines and Solutions for Extending their Residual Lifetimes*." Cigre Session 22-201, 2000.

[14] A.A. Smirnov, P.I. Romanov, "*Database for 330-750 kV transmission line Insulation: Structure, Data Mining, Use for the Purpose of Improvement of Line Operation,*" Cigre Session 15-101, 2002.

[15] G.F. Brennan, *Refurbishment of Existing Overhead transmission lines*." Cigre Session B2-203, 2004, Paris, France.

[16] Thanapong Suwanasri, "*Program Development for Condition and Importance Evaluation of Transmission Line*." Final Report. September, 2018.

[17] Delmo M. Correia, Dalton O. C. Brasil and Dauro C. Lima, *A Proposal for the Evaluation of Transmission Line Performance in a Competitive Market*. Cigre Session 22-104, 2002.

[18] A. Van Der Wal, R.M.A.M. Voncken, "*Extending the Service Life of Aged Overhead Line Towers,*" CIGRE Session B2-212, 2008.

[19] J.C. de Saboia Stephan, C. Ferreira Costa, *Uprate and Upgrade of Overhead Transmission Lines Methodologies and Reliability,*" CIGRE Session B2-202, 2008.

[20] Phillippe Grand, "*The Life Extension Policy of Overhead Lines*," Cigre Session B2-306, 2010.

[21] Cattareeya Suwanasri, Thanapong Suwanasri, Waraporn Luejai, Surapol Saribut, "Cost-benefit for HV transmission line renovation and replacement based on failure probability and risk-based maintenance," *In the Proceedings of the 21st International Symposium on High Voltage Engineering (ISH 2019)*, Budapest, Hungary.

[22] Cigre, "*International Survey of Component Costs of Overhead transmission lines*," Cigre Electra no. 137, 1991.

Improvement for Voltage Sag with Photovoltaic Performance on Distribution System

Papon Ngamprasert, Sakhon Woothipatanapan,
Poonsri Wannakarn, Nattachote Rugthaicharoencheep*

Department of Electrical Engineering, Faculty of Engineering
Rajamangala University of Technology Phra Nakhon. Bangkok, THAILAND

Abstract: This paper presents an improvement for voltage sag with photovoltaic performance on distribution system. The improvement for the sag voltage is a factor in the efficiency of the power distribution system. Under technical constraints such as power flow and bus voltage limits. Modeling solution that uses the radius 69 bus distribution system with distributed generators (DG). It is therefore proposed in this paper to solve a solar power plant into the power distribution system problem based on a power flow algorithm. The results show that solar power plant can be improvement for voltage sag on distribution system.

***Keyword*—Voltage Sag, Photovoltaic, Distribution System.**

I. INTRODUCTION

DISTRIBUTED generation is an approach that employs small-scale technologies to produce electricity close to the end users of power. DG technologies often consist of modular (and sometimes renewable-energy) generators, and they offer a number of potential benefits. For example, of DG such as wind, solar, fuel cells, hydrogen, and biogas show in Fig.1.

The DGs placement in distribution system to voltage profile improvement by photovoltaic farm on distribution system under the technical conditions, power flow equation, line capability. The experiment with the model of distribution system 69 buses was evaluated to find the answer with the proposed technique.

Voltage sags (or dips-American English uses "sag", and British English uses "dip", but they mean exactly the same thing) are the most common power quality disturbance [1].

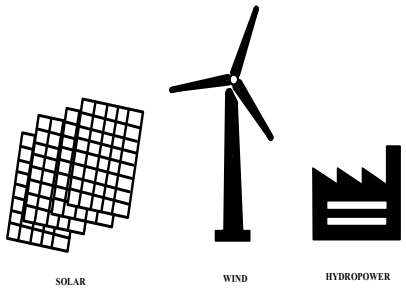

Fig. 1. Type of distributed generation.

This type of disturbance is typically by a short circuit, or fault, on the power distribution grid. The grid, in this case, includes the mains wiring inside the building. Most experts agree that more than 50% of voltage sags are caused by something inside the building. The power supply on this is typical of inexpensive single-phase and three-phase supplies. Supplies like these are found in computers, robots, adjustable speed drives (also called variable frequency drives), etc. Here's how the supply work: a bridge rectifier feeds pulsed DC current to a bulk electrolytic capacity. A Distributed system with DGs installation as show in Fig. 2.

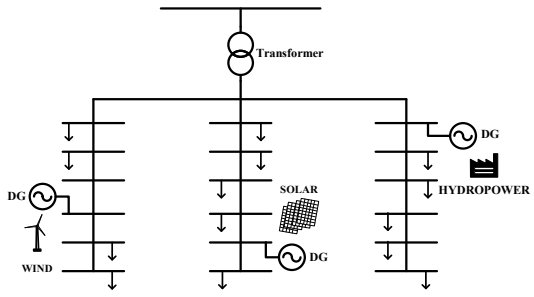

Fig. 2. Distributed system with DGs installation.

Papon Ngamprasert is with the Department of Electrical Engineering, Faculty of Engineering, Rajamangala University of Technology Phra Nakhon, Bangkok, 10800, THAILAND. (phone: 66 890593970; e-mail: papon@ieee.org)

Sakhon Woothipatanapan is with the Department of Electrical Engineering, Faculty of Engineering, Rajamangala University of Technology Phra Nakhon, Bangkok, 10800, THAILAND. (phone: 66 983945539; e-mail: sakhon.w@rmutp.ac.th)

Poonsri Wannakarn is with the Department of Electrical Engineering, Faculty of Engineering, Rajamangala University of Technology Phra Nakhon, Bangkok, 10800, THAILAND. (phone: 66 860049952; e-mail: poonsri.w@rmutp.ac.th)

*Corresponding author: Nattachote Rugthaicharoencheep is with the Department of Electrical Engineering, Faculty of Engineering, Rajamangala University of Technology Phra Nakhon, Bangkok, 10800, THAILAND. (phone: 66 613536426; e-mail: nattachote.r@rmutp.ac.th)

These capacitors are generally available only in certain discrete values-try the slider. A regulator then ensures that the output voltage is a constant, steady, DC value. In this case, the regulator is set for 300V DC, with a minimum forward voltage drop of 60V [2-3]. The nominal input is 240VAC. You can adjust the regulator efficiency.

II. VOLTAGE SAG

The sag voltage is defined as reducing the rms voltage between 10-90% which continues from half a cycle to one minute shown in Fig. 3.

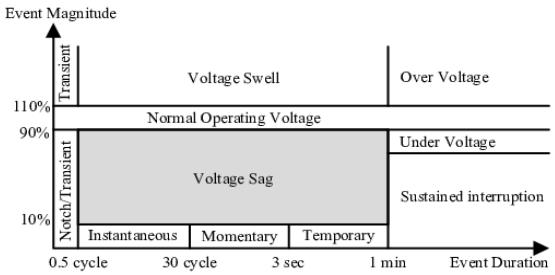

Fig. 3. Voltage Sag/Swell of IEEE Standard.

Most of the voltage sag are caused by a short-circuit to a single-phase ground. The starting of a with high power motor can be also create a voltage sag down shown in Fig. 4.

The maximum and minimum values of voltage at the consumer end are prescribed in I.E. Rules, 1956. Both voltage drop and losses depend on the impedance of the line as well as its loading. Generally, lower-line voltage drop and line losses are desirable and a larger conductor size can be used for that purpose. However, use of a conductor above a certain size yields diminishing returns in terms of voltage drop and losses. Impedance (Z=R + jX) does not drop much where R is already small and further reduction in reactance X is a function of conductor spacing, which does not change with conductor size. Therefore, for any loading an optimum conductor size is desirable.

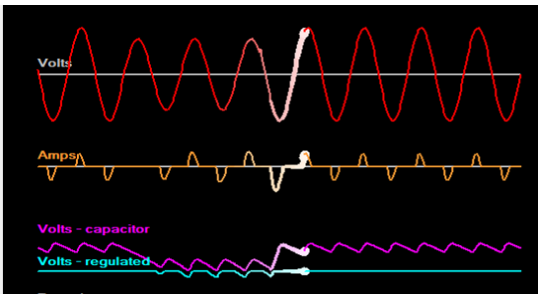

Fig. 4. Voltage Sag.

II. PHOTOVOLTAIC

Solar photovoltaic (PV) power generation uses renewable energy that is natural, safe and sustainable. PV is a device that converts sunlight into electricity using the intensity of solar [4]. PV systems used for many photovoltaic farms connect to the grid everywhere, especially in developed countries with large markets [1]. A schematic diagram of solar photovoltaic (PV) system as show in Fig. 5.

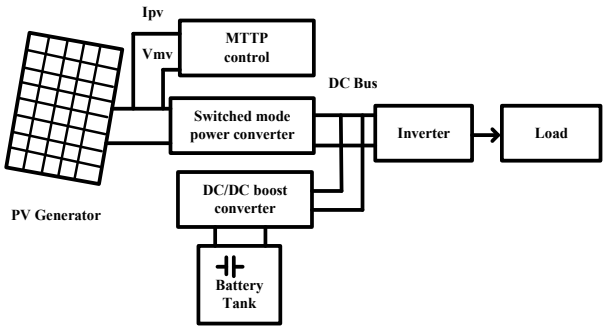

Fig. 5. Schematic diagram of a PV system.

Photovoltaic systems include PV array system which consists of two or more solar panel that converts sun light into electricity. Photovoltaic system is a non-conventional source of energy like wind turbine etc. It is used with dynamic voltage recover (DVR) system for energy storage. This system will provide energy to dc source which is used by inverter system to convert dc energy into ac energy for further applications of DVR system. The equivalent circuit model of photovoltaic cell is shown in Fig. 6 [5].

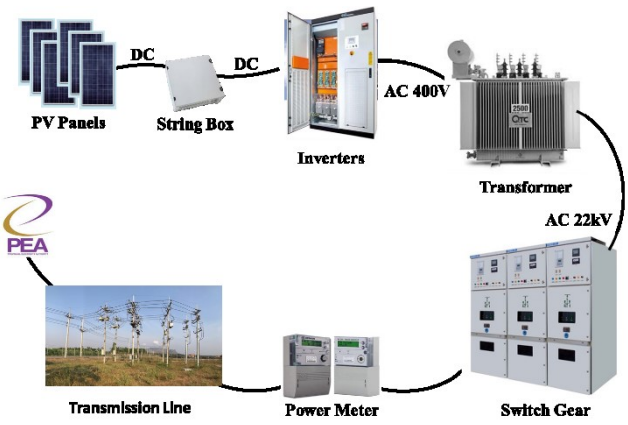

Fig. 6. Photovoltaic systems.

In recent years, all large-scale urban blackouts are due to transmission line overload which connected one or more distribution network with transmission network. Therefore, the energy control strategy which this article designed will satisfy the internal load demand of distribution network in maximal degree. And the thoughts of this strategy are reduced the long-distance power transmission, autarky and superfluous power feeding external. The photovoltaic diesel generator hybrid power supply system will be programmed as isolated island operation model which could access new energy maximum and will running at grid connected mode to send out extra solar energy [6].

Without photovoltaic outputting, if the battery packs output is less than the local load demands the diesel

generators will fully generating. If the battery packs can satisfy load demand, the load will chose using battery backs or diesel engines to undertake the residual load and the criterion is sensitive load. When the photovoltaic fully outputting can't satisfy the load demand, the diesel generators will undertake the surplus load demand. This could avoid get or send energy to distribution network. Therefore, the access number and access positions of photovoltaic diesel generator hybrid power supply system are random. In each access position, the optimizing function can get the optimal access capacity and control model. The equivalent static model of a solar cell by a diode circuit as shown in Fig. 7 [7].

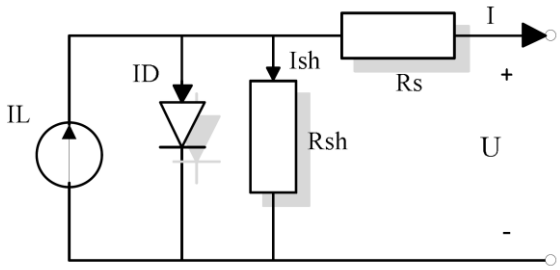

Fig. 7. Equivalent static model of a solar cell

The relation between the output voltage U and the load current can be formulated as follows [8].

$$I = I_L - I_D = I_L - I_O\left[\exp\left(\frac{U + RI_S}{\alpha}\right) - 1\right] \quad (1)$$

Where I is load current

I_L is current photo

I_0 is saturation current

U is output voltage

Rs is series resistor

α is voltage temperature coefficient

II. Formulation

This standard presents definition and table of voltage sag/swell base on categories (instantaneous, momentary, temporary) typical duration, and typical magnitude. The typical residential utility power after sag/swell disturbance is in the range of +/-5% from the nominal of voltage swell [9].

$$Sag(\%) = \frac{V_{pre\ sag} - V_{sag}}{V_{pre\ sag}} \quad (2)$$

$$Swell(\%) = \frac{[V_{pre\ swell} - V_{swell}]}{V_{pre\ swell}} \quad (3)$$

There are two methods for voltage drop (VD) calculations.

$$Maximum\ demand = \frac{Sum\ of\ kVA\ rating\ of\ distribution\ transformers}{Diversity\ factor} \quad (4)$$

$$\%\,VD = \frac{VD\ per\ km.kVA \times (total\ km.kVA)}{Diversity\ factor} \quad (5)$$

$$Demand\ factor = \frac{1.732 \times kV \times maximum\ demand}{Sum\ of\ kVA\ rating\ of\ distribution\ transformers} \quad (6)$$

$$\%\,VD = VD\ per\ km.kVA \times (total\ km.kVA) \times demand\ factor \quad (7)$$

When considering the constant energy factor is the reactive power can be calculate with the equation (8).

$$Q_G = P_G tan\left(cos^{-1}(pf_G)\right) \quad (8)$$

where pf_G is the power factor specified in the DG. Then the injected net current associate at DG.

III. Solution Methodology

The Tabu search algorithm is applied to solve the voltage sag problem using the following steps for calculation.

Step 1: Read the bus, load and branch data of a distribution system including all the operational constraints.

Step 2: Randomly select a feasible solution from the search space: $S_0 \in \Omega$. The solution is represented by the switch number that should be opened during network reconfiguration.

Step 3: Set the size of a Tabu list, maximum iteration and iteration index $m = 1$.

Step 4: Let the initial solution obtained in step 2 be the current solution and the best solution: $S_{\text{best}} = S_0$, and $S_{\text{current}} = S_0$.

Step 5: Perform an optimal power flow by a MATPOWER software package [10] to determine power loss, bus voltages, branch currents and generation schedules of the distributed generators.

Step 6: Calculate the total power loss using (1) and check whether the current solution satisfies the constraints. A penalty factor is applied for constraint violation.

Step 7: Calculate the aspiration level of S_{best}: $f_{\text{best}} = f(S_{\text{best}})$. The aspiration level is the sum of L and a penalty function

Step 8: Generate a set of solutions in the neighborhood of S_{current} by changing the switch numbers that should be opened. This set of solutions is

designated as S_{neighbor} .

Step 9: Calculate the aspiration level for each member of S_{neighbor} , and choose the one that has the highest aspiration level, $S_{\text{neighbor\_b est}}$.

Step 10: Check whether the attribute of the solution obtained in step 9 is in the Tabu list. If yes, go to step 11, or else $S_{\text{current}} = S_{\text{neighbor\_b est}}$ and go to step 12.

Step 11: Accept $S_{\text{neighbor\_b est}}$ if it has a better aspiration level than f_{best} and set $S_{\text{current}} = S_{\text{neighbor\_b est}}$, or else select a next-best solution that is not in the Tabu list to become the current solution.

Step 12: Update the Tabu list and set $m = m + 1$.

Step 13: Repeat steps 8 to 12 until a specified maximum iteration has been reached.

Step 14: Repeat step 5 and report the optimal solution.

Distribution system with DG as show in Fig. 8.

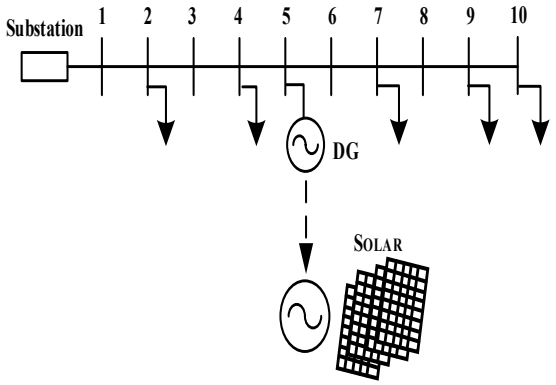

Fig. 8. Distribution system with DG.

IV. CASE STUDY

For the study, improve the voltage profile using 69 buses distribution system model with DG as shown in Fig.9. The nine DG units are located at buses 19, 29, 36, 39, 49, 53, 59, 62 and 69 have the capacity of 300, 400, 100, 100, 100, 400, 100, 400, 200 and 200 kW respectively. The total installed capacity of DGs is 1,000 kW. The system base 100 MVA and voltage base is 12.66 kV.

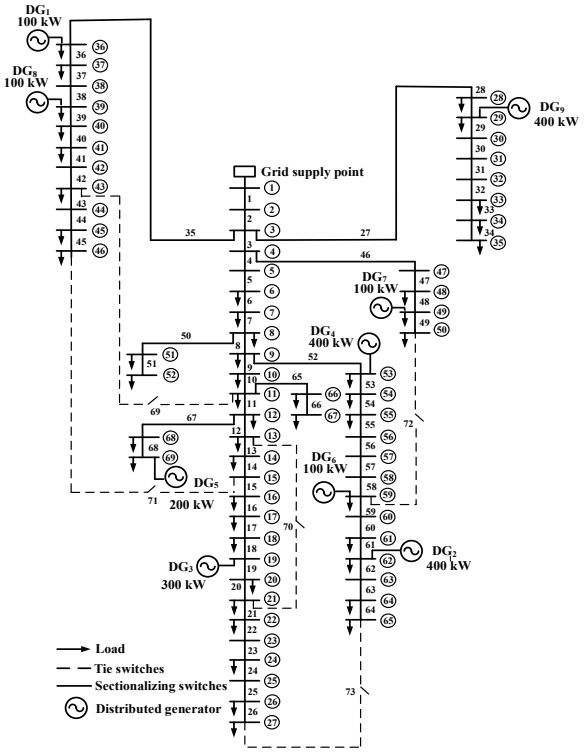

Fig. 9. Single-line diagram of 69-bus distribution system.

Each branch in the system has a separate switch to reconfigure. The data loaded in the AI table and AII table provide branch information [11].

The switch number 1-68 is sectionalizing switches on a distribution feeder (normally close) and switch number 69-73 is tie switches (normally open). The total load for this test system is 3,801.89 kW and 2,694.10 kVAr. The voltages all buses are set at 0.95 and 1.05 p.u.

Three cases are examined as follows:

Case 1: Without DGs in distribution system. This case represents the base case.

Case 2: Installation DGs 5 buses in distribution system.

Case 3: Installation DGs 9 buses in distribution system.

X. RESULTS

The numerical results for the 3 cases are shown in Fig. 10, 11 and 12 the bus voltages of all buses for cases 1, 2 and 3. As can be seen, the bus voltages are improved in the presence of the DGs.

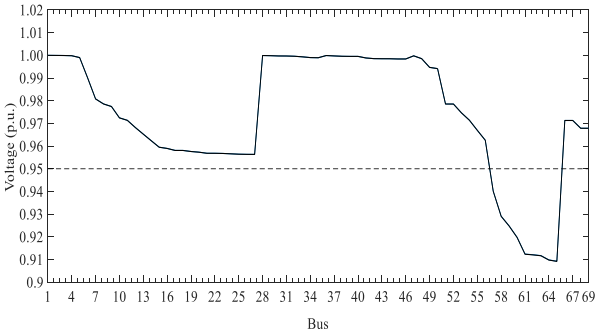

Fig. 10. Without in distribution system.

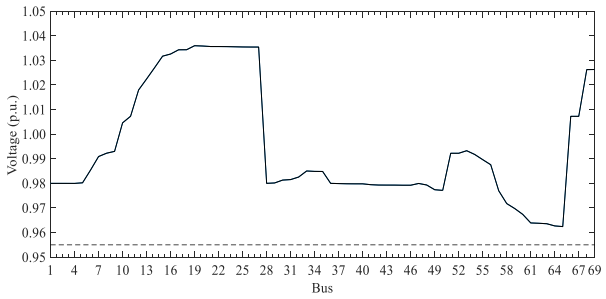

Fig. 11. Installation DGs 5 buses in distribution system.

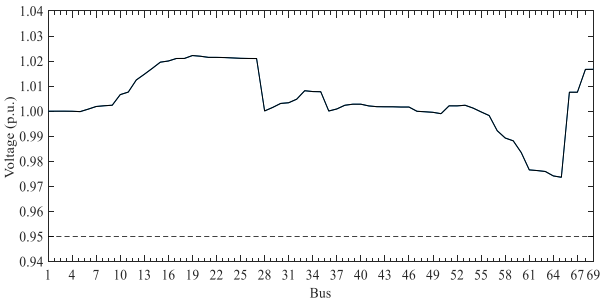

Fig. 12. Installation DGs 9 buses in distribution system.

XI. Conclusion

This paper presents an improvement for voltage sag with photovoltaic performance on distribution system. Tested with a single-line diagram of 69-bus distribution system, which has performed three cases is examined as follows, Case 1: Without in distribution system, Case 2: Installation DGs 5 buses in distribution system, Case 3: Installation DGs 9 buses in distribution system. It was found that Case 1: Without in distribution system does not improve distribution system. But Case 2: Installation DGs 5 buses in distribution system, Case 3: Installation DGs 9 buses in distribution system.

Acknowledgment

The author would like to express his sincere thanks to the Rajamangala University of Technology Phra Nakhon (RMUTP), Thailand for supporting.

References

[1] F. Sarkar, and R. Ramya, “Voltage sag and distortion mitigation in a hybrid power system using FACTs device,” International Journal of Science and Research, vol.4, no.5, pp.311 - 317, May 2015.

[2] Y. Zheng, Z. Y. Dong, K. Meng, H. Yang, M. Lai, and K. P. Wong, “Multi-objective Distributed Wind Generation Planning in an Unbalanced Distribution System,” CSEE Journal of Power and Energy Systems, vol.3, no.2, pp.186-195, June 2017.

[3] V. Vai, M.-C. Alvarez-Herault, B. Raison, and L. Bun, “Optimal Low-voltage Distribution Topology with Integration of PV and Storage for Rural Electrification in Developing Countries: A Case Study of Cambodia,” Journal of Modern Power Systems and Clean Energy, vol.8, no.3, pp.531-539, May 2020.

[4] R. K. Varma, S. A. Rahman, V. Atodaria, S. Mohan, and T. Vanderheide,“Technique for Fast Detection of Short Circuit Current in PV Distributed Generator,” IEEE Power and Energy Technology Systems Journal, vol.3, no.4, pp.155-165, December 2016.

[5] S. Aarif, and Er. R. K. Randhawa, “Improvement of power quality using photovoltaic dynamic voltage restorer,” International Journal for Research in Applied Science & Engineering Technology, vol.5, no.9, pp.703-708, September 2017.

[6] GE Yang-yang, CAI Zhi-yuan, and SUN Li-yong, “Optimal placement for hybrid energy in micro-grid,” IEEE International Conference on Power System Technology (POWERCON), 2016.

[7] O. Z. Nezhad, S. A. Hashemi Zadeh, M. Mohammadian, and A. A. Gharaveisi, “The analysis of hybrid system as dg in smart grids by the use of loss sensitivity coefficient method,” Smart Grid Conference (SGC), December 2013.

[8] M. Cortés-Carmona, J. Vega, and M. Cortés-Olivares,“Power flow algorithm for analysis of distribution networks including distributed generation,” IEEE PES Transmission & Distribution Conference and Exhibition - Latin America (T&D-LA), Lima, Perú, pp.1-5, 2018.

[9] A. Kiswantono, E. Prasetyo, and A. Amirullah, “Comparative Performance of Mitigation Voltage Sag/Swell and Harmonics Using DVR-BES-PV System with MPPT-Fuzzy Mamdani/MPPT-Fuzzy Sugeno,” International Journal of Intelligent Engineering and Systems, vol.12, no.2, pp.222-235, April 2019.

[10] R. D. Zimmerman, C. E. Murillo-Sánchez, and D. Gan, “A MATPOWERTM power system simulation package version 3.1b2”, Power Systems Engineering Research (PSERC), September, 2006.

[11] J. S. Savier, and D. Das,“Impact of network reconfiguration on loss allocation of radial distribution systems,” IEEE Trans. on Power Delivery, vol.22, no.4, pp.2473-2480, October 2007.

Appendix

TABLE AI
Load Data of 69-Bus Distribution System

Bus Number	P_L (kW)	Q_L (kVAr)	Bus Number	P_L (kW)	Q_L (kVAr)
6	2.60	2.20	37	26.00	18.55
7	40.40	30.00	39	24.00	17.00
8	75.00	54.00	40	24.00	17.00
9	30.00	22.00	41	1.20	1.00
10	28.00	19.00	43	6.00	4.30
11	145.00	104.00	45	39.22	26.30

TABLE AI (Continued)

Bus Number	P_L (kW)	Q_L (kVAr)	Bus Number	P_L (kW)	Q_L (kVAr)
12	145.00	104.00	46	39.22	26.30
13	8.00	5.00	48	79.00	56.40
14	8.00	5.50	49	384.70	274.50
14	8.00	5.50	49	384.70	274.50
16	45.50	30.00	50	384.70	274.50
17	60.00	35.00	51	40.50	28.30
18	60.00	35.00	52	3.60	2.70
20	1.00	0.60	53	4.35	3.50
21	114.00	81.00	54	26.40	19.00
22	5.00	3.50	55	24.00	17.20
24	28.00	20.00	59	100.00	72.00
26	14.00	10.00	61	1,244.00	888.00
27	14.00	10.00	62	32.00	23.00
28	26.00	18.60	64	227.00	162.0
29	26.00	18.60	65	59.00	42.00
33	14.00	10.00	66	18.00	13.00
34	19.50	14.00	67	18.00	13.00
35	6.00	4.00	68	28.00	20.00
36	26.00	18.55	69	28.00	20.00

TABLE AII
BRANCH DATA OF 69-BUS DISTRIBUTION SYSTEM

Branch Number	Sending end bus	Receiving end bus	R (Ω)	X (Ω)
1	1	2	0.0005	0.0012
2	2	3	0.0005	0.0012
3	3	4	0.0015	0.0036
4	4	5	0.0251	0.0294
5	5	6	0.3660	0.1864
6	6	7	0.3811	0.1941
7	7	8	0.0922	0.0470
8	8	9	0.0493	0.0251
9	9	10	0.8190	0.2707
10	10	11	0.1872	0.0619
11	11	12	0.7114	0.2351
12	12	13	1.0300	0.3400
13	13	14	1.0440	0.3450
14	14	15	1.0580	0.3496
15	15	16	0.1966	0.0650
16	16	17	0.3744	0.1238
17	17	18	0.0047	0.0016
18	18	19	0.3276	0.1083
19	19	20	0.2106	0.0690
20	20	21	0.3416	0.1129
21	21	22	0.0140	0.0046
22	22	23	0.1591	0.0526
23	23	24	0.3463	0.1145
24	24	25	0.7488	0.2475
25	25	26	0.3089	0.1021
26	26	27	0.1732	0.0572
27	3	28	0.0044	0.0108
28	28	29	0.0640	0.1565
29	29	30	0.3978	0.1315
30	30	31	0.0702	0.0232
31	31	32	0.3510	0.1160
32	32	33	0.8390	0.2816
33	33	34	1.7080	0.5646
34	34	35	1.4740	0.4873
35	3	36	0.0044	0.0108
36	36	37	0.0640	0.1565
37	37	38	0.1053	0.1230
38	38	39	0.0304	0.0355
39	39	40	0.0018	0.0021
40	40	41	0.7283	0.8509
41	41	42	0.3100	0.3623
42	42	43	0.0410	0.0478
43	43	44	0.0092	0.0116
44	44	45	0.1089	0.1373
45	45	46	0.0009	0.0012
46	4	47	0.0034	0.0084

TABLE AII (CONTINUED)

Branch Number	Sending end bus	Receiving end bus	R (Ω)	X (Ω)
47	47	48	0.0851	0.2083
48	48	49	0.2898	0.7091
49	49	50	0.0822	0.2011
50	8	51	0.0928	0.0473
51	51	52	0.3319	0.1114
52	9	53	0.1740	0.0886
53	53	54	0.2030	0.1034
54	54	55	0.2842	0.1447
55	55	56	0.2813	0.1433
56	56	57	1.5900	0.5337
57	57	58	0.7837	0.2630
58	58	59	0.3042	0.1006
59	59	60	0.3861	0.1172
60	60	61	0.5075	0.2585
61	61	62	0.0974	0.0496
62	62	63	0.1450	0.0738
63	63	64	0.7105	0.3619
64	64	65	1.0410	0.5302
65	11	66	0.2012	0.0611
66	66	67	0.0047	0.0014
67	12	68	0.7394	0.2444
68	68	69	0.0047	0.0016
Tie line				
69	11	43	0.5000	0.5000
70	13	21	0.5000	0.5000
71	15	46	1.0000	0.5000
72	50	59	2.0000	1.0000
73	27	65	1.0000	0.5000

IEET Editorial Office

EEAAT - Electrical Engineering Academic Association (Thailand)
Room 409, F-Building
140 Cheum-Sampan Rd.
Nong Chok, Bangkok, Thailand 10530
Tel: +662-988-3655 ext 2216 Fax: +662-988-4026

www.journal.eeaat.or.th